Iowa State University
Digital Repository

Retrospective Theses and Dissertations | Iowa State University Capstones, Theses and Dissertations

2005

Study of nano-crystalline silicon deposited by VHF-PE CVD for solar cell devices

Puneet Sharma
Iowa State University

Follow this and additional works at: https://lib.dr.iastate.edu/rtd

Part of the Electrical and Electronics Commons

Recommended Citation

Sharma, Puneet, "Study of nano-crystalline silicon deposited by VHF-PE CVD for solar cell devices " (2005). *Retrospective Theses and Dissertations*. 1771.
https://lib.dr.iastate.edu/rtd/1771

This Dissertation is brought to you for free and open access by the Iowa State University Capstones, Theses and Dissertations at Iowa State University Digital Repository. It has been accepted for inclusion in Retrospective Theses and Dissertations by an authorized administrator of Iowa State University Digital Repository. For more information, please contact digirep@iastate.edu.

المنارة للاستشارات

www.manaraa.com

Study of nano-crystalline silicon deposited by VHF-PE CVD for solar cell devices

by

Puneet Sharma

A dissertation submitted to the graduate faculty

in partial fulfillment of the requirements for the degree of

DOCTOR OF PHILOSOPHY

Major: Electrical Engineering

Program of Study Committee:
Vikram L. Dalal, Major Professor
Gary Tuttle
Rana Biswas
Joseph Shinar
Mani Mina

Iowa State University

Ames, Iowa

2005

Copyright © Puneet Sharma, 2005. All rights reserved.

UMI Number: 3200458

INFORMATION TO USERS

The quality of this reproduction is dependent upon the quality of the copy submitted. Broken or indistinct print, colored or poor quality illustrations and photographs, print bleed-through, substandard margins, and improper alignment can adversely affect reproduction.

In the unlikely event that the author did not send a complete manuscript and there are missing pages, these will be noted. Also, if unauthorized copyright material had to be removed, a note will indicate the deletion.

UMI®

UMI Microform 3200458

Copyright 2006 by ProQuest Information and Learning Company.

All rights reserved. This microform edition is protected against unauthorized copying under Title 17, United States Code.

ProQuest Information and Learning Company
300 North Zeeb Road
P.O. Box 1346
Ann Arbor, MI 48106-1346

Graduate College
Iowa State University

This is to certify that the doctoral dissertation of

Puneet Sharma

has met the dissertation requirements of Iowa State University

Signature was redacted for privacy.

Major Professor

Signature was redacted for privacy.

For the Major Program

TABLE OF CONTENTS

ABSTRACT vi

CHAPTER 1: INTRODUCTION 1

CHAPTER 2: LITERATURE REVIEW 5

1. Understanding the material 5
2. Growth regime 11
3. Effect of impurities 11
4. Effect of temperature 11
5. High efficiency devices 13

CHAPTER 3: MATERIAL GROWTH AND CHARACTERIZATION 15

1. Sample preparation 15
2. VHF reactor 17
3. Characterization techniques 18
    A. Thickness 19
    B. IV analysis 20
    C. Quantum efficiency 20
    D. Measurement of doping and defect densities 22
    E. Measurement of diffusion length of holes 23

F. Structural analysis 24

1. Raman analysis 24

2. XRD analysis 25

CHAPTER 4: RESULTS AND DISCUSSION 27

1. Effect of ppm levels of Boron and Phosphine 27

2. Relationship between deep defects and net doping 30

3. Measurement of diffusion length of minority carriers (holes) and deep defect density 31

4. Measurement of location of trap levels 32

5. Dark IV curves and crystallinity 34

6. Effect of Hydrogen dilution 36

7. Use of graded ppm B doping to improve carrier collection 38

8. Improving voltage by the use of an interfacial capping or buffer layer between the p and the n layers 41

9. Improving fill factors by reducing series resistance 43

10. Influence of seed layers on crystallinity and device performance 44

11. Controlling crystallinity and device properties by dilution with Helium 46

12. Influence of deposition temperature on device properties 46

13. Influence of Oxygen on device properties 48

14. Influence of baking of the reactor walls on defect densities 50

15. Other data relevant to this work 51

CHAPTER 5: CONCLUSIONS 55

FUTURE WORK 57

REFERENCES 58

ACKNOWLEDGEMENTS 61

APPENDIX A 62

APPENDIX B 64

ABSTRACT

Nanocrystalline Silicon (nc-Si: H) is an important material for photovoltaic energy conversion dev ices and for thin film transistors. The material consists of small grains of Si, of the order of 10-20 nm, with a significant amorphous phase and bonded Hydrogen (H) interspersed between the grains. Their presence serves to passivate the grain boundaries and reduces the recombination at the boundaries which lead to reasonably good electronic transport in the device. Hence material can be used for applications in photovoltaic cells (which depend upon efficient collection of minority carriers) and thin film transistors, which require good electron and hole mobilities.

What has not been done previously is a systematic study of the fundamental material properties in a device-type structure and the relationship between these properties and the processing conditions. The transport properties in transverse direction, measured in films deposited on glass substrates are very different from the properties in the vertical direction measured in films deposited on stainless steel substrates. Hence our research is involved with studies on the device type structures.

In this work, a systematic study is carried out of midgap defect densities and minority carrier diffusion lengths in nanocrystalline p+nn+ devices by changing the doping and defect densities with different techniques. The devices and films were grown using mixtures of silane and hydrogen in a VHF diode plasma discharge. Parameters such as temperature, pressure and hydrogen/silane ratios were systematically varied to produce films with different crystallinity and native donor concentration. Defect densities were measured and the energetic location of the traps was found to be approximately 0.5 to 0.35 eV below the conduction band. A surprising finding was that there was a 1:1 correlation between the deep defect states which were responsible for carrier capture, and the donor density. The diffusion length were measured and showed an excellent correlation with the deep defect density, approximately following the Shockley-Read-Hall recombination model which is the first experimental validification of the theoretical model.

Special samples were also prepared for measurement of mobility using space charge limited current techniques in n+nn+ devices, and for measurement of carrier lifetimes using reverse recovery techniques. These measurements, by other students in the group, showed that the mobility of electrons was in the range of 1 cm^2/V-s and that hole lifetimes were in the range of few hundred nanoseconds. When the measured hole lifetimes were plotted against the inverse of the defect densities measured in these very small devices, an approximate linear correlation was obtained, thus verifying the SRH recombination model. The simultaneous measurement of diffusion length in these very same samples yielded an estimate for the hole mobility.

Also Dark I-V current studies on these devices were done and their relationship with crystallinity was studied which was backed by Quantum Efficiency measurements. Two techniques of graded TMB and H_2 were used to improve hole transport in these devices. A final device innovation was to study the use of a thin a-Si: H buffer layer between the n base layer and the p+ junction layer which significantly improved the open circuit voltage, presumably by reducing the recombination at the interface states.

Thus, we have been able to make measurements of the important fundamental material properties, electron and hole mobility, defect density, minority carrier lifetime and minority carrier diffusion length, all in the same or very similar samples. This is the first time ever that such systematic measurements have been made in this material system.

CHAPTER 1

INTRODUCTION

Nanocrystalline Silicon (nc-Si: H) is a heterogeneous material of crystalline grains and the amorphous tissue. The grains can have sizes that can vary from couple of nanometer's (nm's) to hundred's of nm's. The grains are surrounded by grain boundaries which are saturated with Hydrogen (H) or with thin a-Si: H tissue. The presence of significant H bonding at the grain boundaries, and the presence of the thin amorphous tissue, lead to excellent minority carrier transport through the grains and minimize grain boundary recombination. Another big effect on the transport is the arrangement of grain aggregates or possibly column's, separated by grain boundaries causing anisotropy in the transport and/or depth profile of the transport properties. Unlike amorphous silicon which has a short ranger order, nc-Si: H has small crystallites within the amorphous tissue and crystallite size increases as the thickness increases, thus showing a localized order.

In 1968 Veprek and Marecek[1] succeeded for the first time with the deposition of hydrogenated microcrystalline silicon (mc-Si: H) fabrication. (Note: Both mc-Si: H and nc-Si: H have been used as synonyms in all the literature. What was initial called microcrystalline silicon with size below 100nm was named Nanocrystalline by Federal Regulation and NSF). Initial applications of microcrystalline silicon (mc-Si) were restricted to its use as p-layers for p-i-n devices because of its high conductivity and high transparency. Its application for Thin-Film Transistors (TFT) was also proposed but never followed seriously until lately because of the following reasons:

1) It was assumed that nc-Si: H has high defect density and therefore cannot be used as photovoltaically active layer in a solar cell device.
2) The strong n-type character was generally observed in as deposited undoped nc-Si: H which led to poor electronic properties (hole lifetimes and poor mobilities).
3) There were doubts about the bandgap of nc-Si: H as compared to crystalline Silicon because of higher absorption with nc-Si.

4) The long fabrication times with 'standard' PECVD deposition techniques, with reported deposition rates below 1 A/sec, was too low for depositing thicker layers.

5) Since nc-Si: H is an indirect bandgap material, higher thickness of i- layer is required for effective absorption around 5-10 μm.

Due to the excellent optoelectronic properties that can be obtained with improved deposition methods like very high frequency glow discharge (VHF–GD) and Hot-Wire with PECVD, (nc-Si: H) has been experiencing a new wave of interest in the scientific community. Substantial amount of research is being done to understand the material and electrical properties of nc-Si along with its structure and deposition trends for which simulation and modeling studies are being conducted by different groups.

Motivation for understanding this material comes from the facts that:

1) The nc-Si: H shows a very little light induced degradation which has hampered the use of amorphous silicon as commercial material thus far.

2) Low temperature deposition for obtaining good quality material (~200C) is completely compatible with the amorphous deposition, unlike crystalline silicon. Low temperature processing also gives flexibility of using cheaper substrates like plastics and organic substrates.

3) Higher absorption coefficient in the infrared range, because of it lower band gap can be used effectively as a bottom layer to amorphous layer for efficient trapping of the whole solar spectrum in the so called 'Micromorph' solar cells. The band gap of nc-Si is comparable to crystalline silicon and the increased absorption of nc-Si compared to crystalline silicon can be attributed to the light scattering at the grain boundaries as has been shown[2, 3] in the Figure [1.1 & 1.2].

4) High conductivity and high transparency has lead to its use in p layers for p-i-n/ n-i-p device type structures.

5) Since there is a lower density of valence band tail states, nc-Si gives higher carrier concentration which can be used to make p-channel TFT's.

6) Higher mobility as compared to amorphous Silicon is major advantage for operating speed.

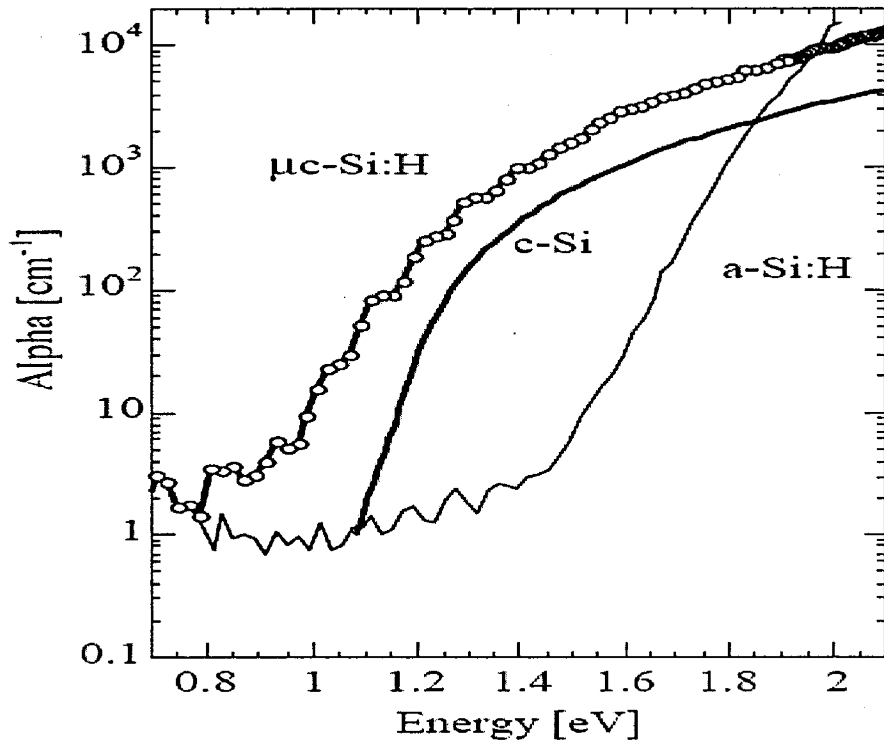

Figure [1.1]: Absorption of nc-Si[3]

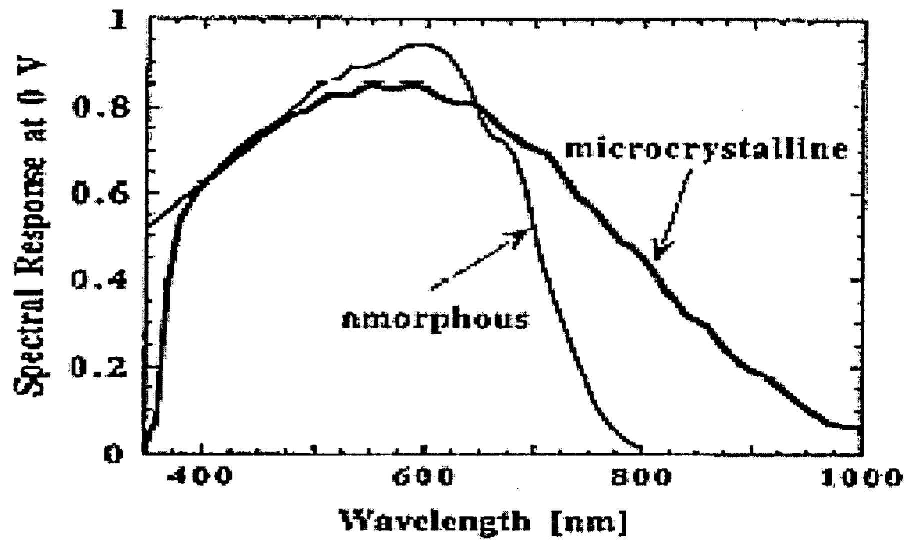

Figure [1.2]: Spectral response vs. Wavelength[2]

Before we dig deep into literature and research done, its worthwhile to mention the objectives of this research as the things to follow have been done keeping these objectives in mind. The objectives have been stated below:

1. To measure donor and deep defect densities in nc-Si: H devices prepared under various deposition conditions and establish a correlation between growth and donor and defect densities
2. To measure fundamental device-related property, diffusion length of holes and to establish whether the transport is controlled by field (as in a-Si: H devices) or by diffusion (as in crystalline Si devices).
3. To change the donor and defect densities
4. To study the correlation between defect densities and diffusion lengths and from that, to study what the recombination mechanism is.
5. To provide device-type samples for measurement of other important parameters, such as mobilities and carrier lifetimes, to others in the group, so that complementary measurements can be made on the same or very similar samples. Also, to correlate results from complementary measurements with the conclusions drawn from my measurements of defect densities, donor densities and diffusion lengths. From these measurements, establish values for some other fundamental parameters, such as capture cross sections of traps in this material.
6. To study the Dark I-V curves in the device and see if they agree with the recombination mechanisms identified above.
7. To design and fabricate improved devices, by using dopant grading techniques and by using amorphous interfaces to reduce recombination at the p-n interface.

CHAPTER 2

LITERATURE REVIEW

1. Understanding the material:

For large scale application of photovoltaics (PV), it is imperative to reduce the manufacturing cost of PV modules by a factor of 2-3 compared to wafer based crystalline silicon wafer based technology. Thin film solar cells have been keen area of research involving different forms and materials of Silicon, CdTe, Cu (In, Ga)Se_2 and many others. While amorphous silicon has been studied and understood a lot, it still suffers from problems of low efficiency and Stabler- Wronski-Effect.

In 1994 the research group at IMT, Neuchetal Switzerland introduced a new photovoltaic material with low defects and moderation conversion efficiency called 'Microcrystalline silicon' named due to its small crystal size. Since then lot of studies have been done on the growth of the material and deposition techniques. However there is a lot that we still that we donot understand about the material for getting its best use.

The deposition and transport quality of nc-Si is a big function of the substrate and deposition conditions[4] used. The low temperature processing allows for using different cheap substrates including plastic substrates, stainless steel and glass substrates. These crystalline silicon films are usually preceded by a-Si layer[5-8] and the crystallinity of the material and grain size are a strong function of the preceding layer. The material is known to have anisotropic behavior in the transport properties. Hence it is very important to understand the transport in both parallel and perpendicular directions to the substrate, although for photovoltaic applications it is important to know the properties in the direction of the growth. AFM studies have shown, done parallel to the surface, two types of grain boundaries – small and large. The small ones are 20- 30 nm big while the large GB's (agglomerates of smaller ones) are 200-300 nm. It has been shown[9-10] that there are 10^{18} grains and only 10^{16} defects. Therefore It has been assumed that these small grains and their grain boundaries are defect free and these boundaries whether they are a-Si tissue or titled boundaries[11, 12] donot adversely affect the band like - transport properties. This idea was independently confirmed

by pico-second laser induced grating[13]. It has been proposed that the role of Large Grain (LG) boundaries is that all the defects and impurities like C, N,O or even H segregate to LG boundaries formed by a-Si tissue, whose mobility gap increase with alloying. At this point sharp decrease in σ_0 (conductivity pre-factor) is found which has been explained by potential barrier formed at the boundaries. This limits the dominant transport to hopping conduction through the tail states below the conduction band. Kocka[4] has similarly shown the growth in the form of cones forming large grain boundaries formed by agglomeration of small grains as seen in the Fig [2.1].

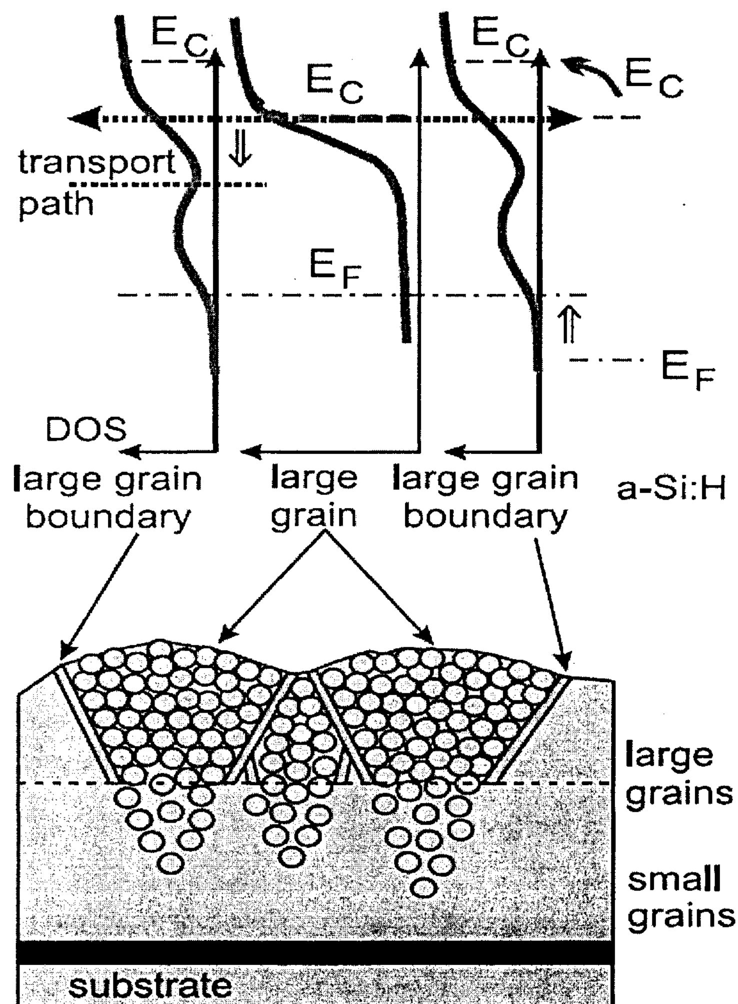

Fig 2.1: Grain Boundaries and growth model by kocka[4]

Hamakawa and Takakura[14] have shown the device simulations for the transport of microcrystalline silicon solar cells and found that the interface states are found at the grain boundaries along with the a-Si tissue. Because of the broad electronic state distribution is given at the GB (Grain boundary), potential has a peak in the conduction band and valley in the valence band as shown in the Figure [2.2]. This potential barrier is measured as the activation energy in the microcrystalline films.

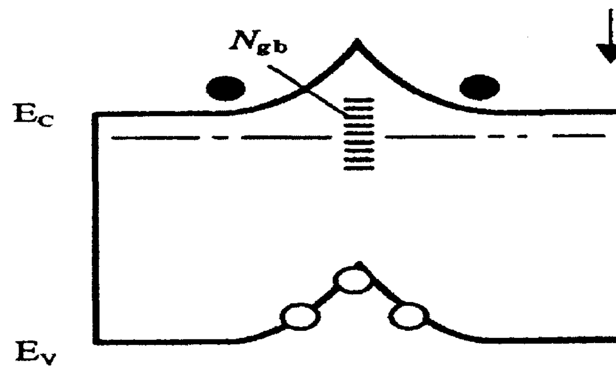

Figure [2.2]: Band profiling at GB[14].

Collins[15] proposed that microcrystalline nuclei originate in the (a -> a + nc) transition layer and act as seeds for the growth of crystals whose size increases with the thickness of the film

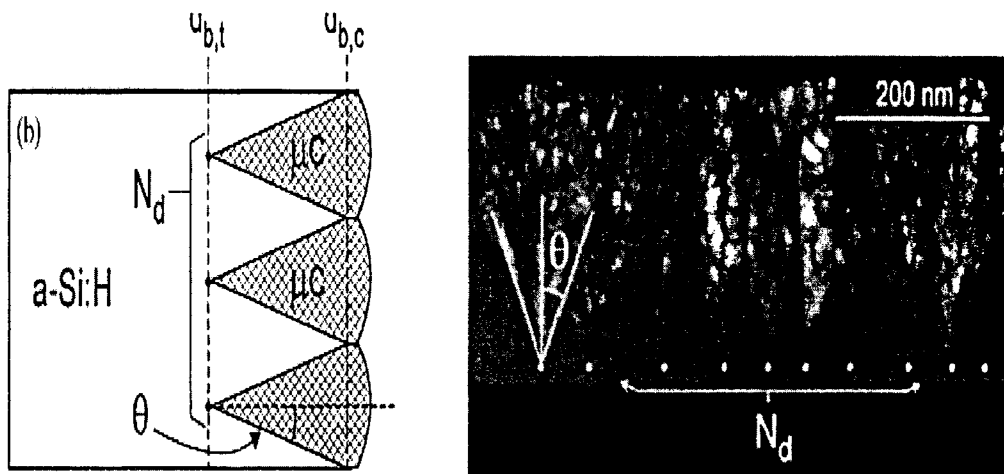

Figure [2.3]: TEM pictures supporting the cone growth model and the seed layers that help in growth of microcrystalline silicon used as seed layer[15].

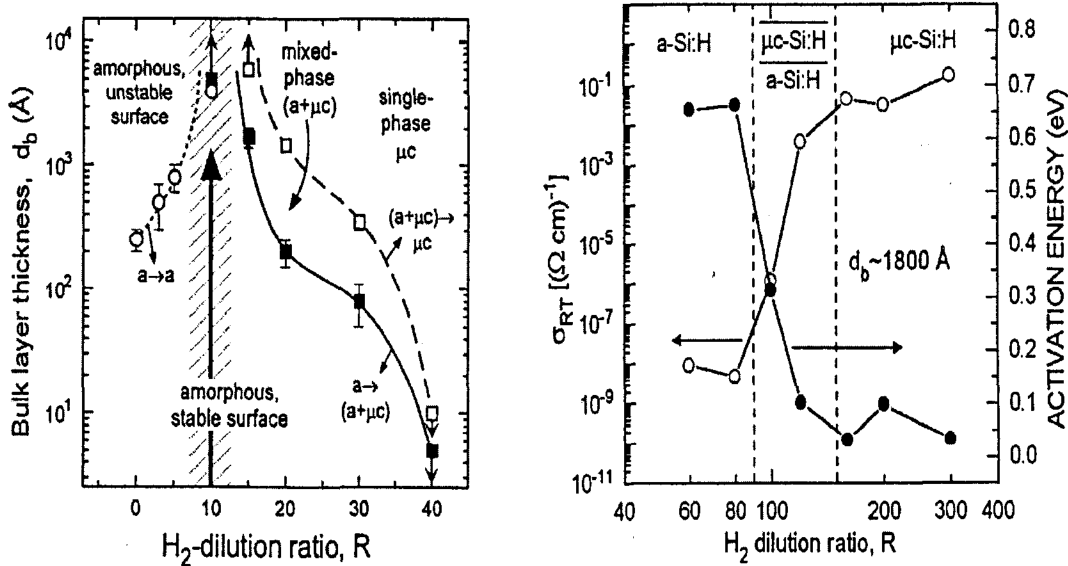

Figure [2.4]: Different regions of growth depending on dilution ratios[15]

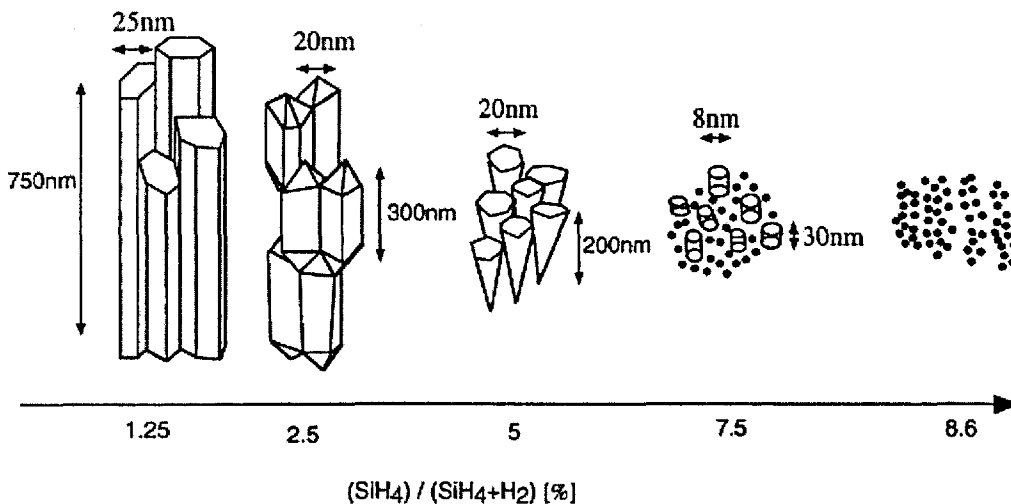

Figure [2.5]: Different types and size of crystals that can be formed[16]

It has been shown that the microcrystalline grain size is a strong function of the ratio SC = SiH_4/SiH_4+H_2 and also the thickness of the film. Crystalline grain size can be estimated by broadening the X-ray diffraction peaks using the Debye-Scherrer equation. As the H_2 dilution is lowered in SiH_4, the open circuit voltage of the devices is expected to increase and

the crystalline fraction would decrease. This effect has been seen in films as shown below[17] in Figure [2.6].

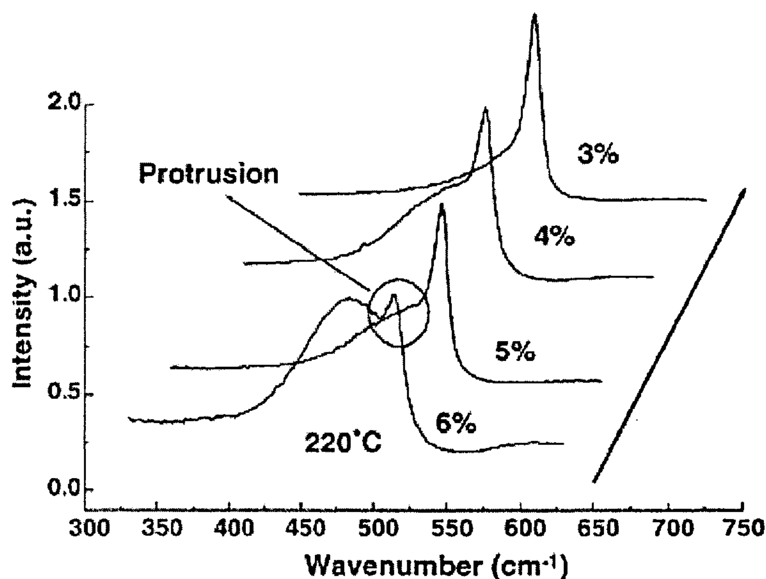

Figure [2.6] Varying Raman Intensity peaks for different SC's[17]

Until recently 13.56 MHz has been the driving frequency but with the requirement of getting better grain sizes and faster deposition rates other methods of deposition are being studied including VHF (Very High Frequency) , Hot-Wire and few other CVD methods. In 1987 IMT, Neuchetal, introduced a new method of deposition know as Very High Frequency "VHF" plasma enhanced CVD method[18]. Using higher plasma excitation frequencies, it has been shown that the deposition rate increases by 5-10 times by various research groups[19-21].

Also using the higher frequency gives better quality microcrystalline layers due to lower energy ion bombardment on the growing surface. The thinner plasma sheaths obtained at higher frequencies lead to lower sheath potential and hence ion bombardment on the growing layer is reduced. The r.f power also gets more efficiently coupled-in into the bulk plasma and hence higher electron densities and better SiH_4 dissociation in bulk plasma is possible as well as increased radical and ion flux on to the growing surface can be achieved at moderate sheath voltages.

It is useful to note that the increase in frequency also drives plasma non-uniformities due to several electromagnetic effects: the skin effect, edge effects and the standing wave conditions.

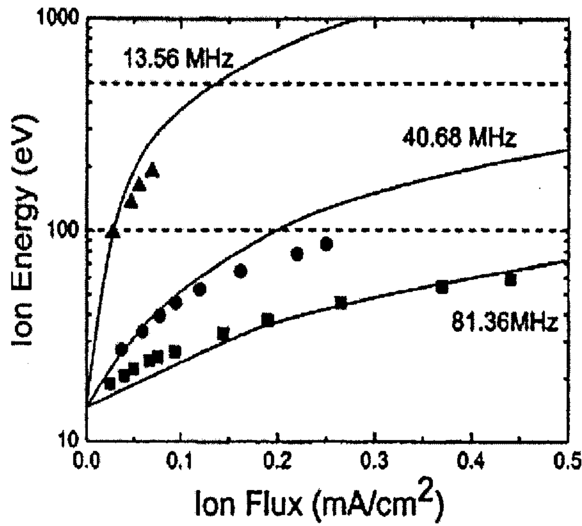

Figure [2.7]: Ion Energy vs. Ion flux for different frequencies

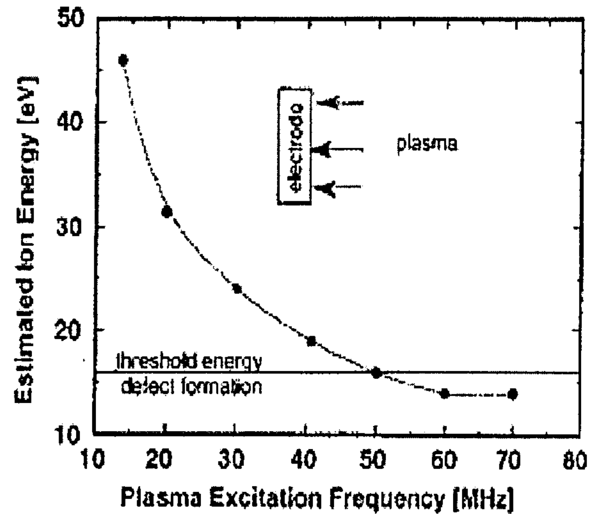

Figure [2.8]: Decreasing Ion Energy with increasing frequency[23]

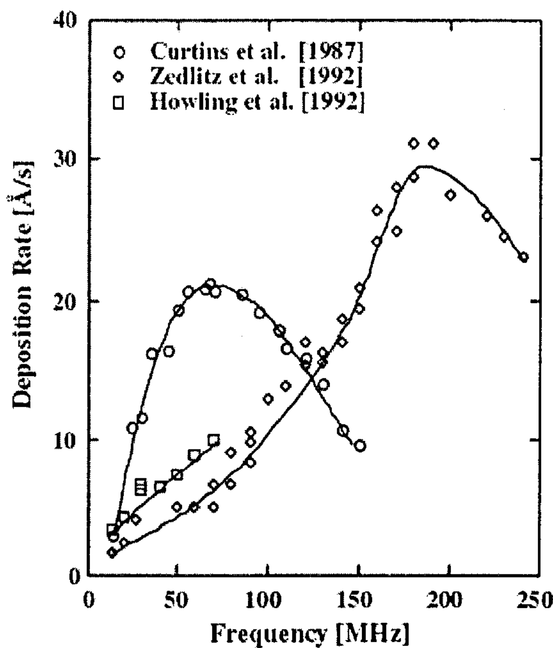

Figure [2.9]: Deposition rate Vs. Frequency

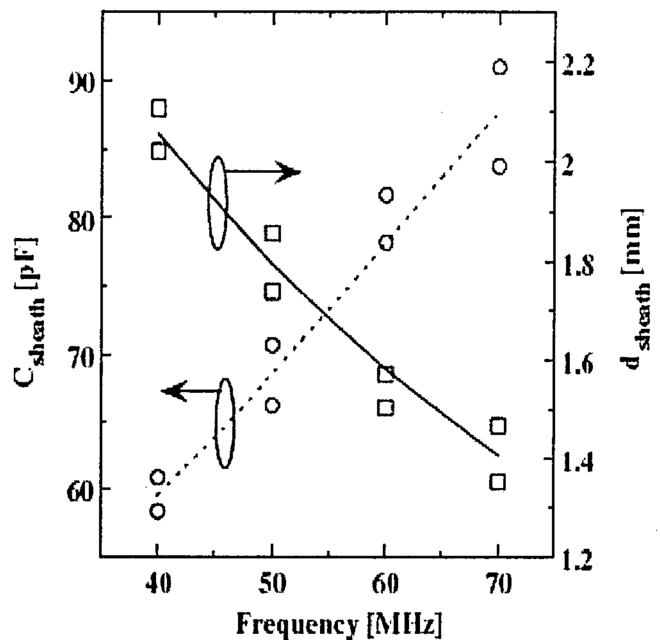

Figure [2.10]: Sheath Potential vs. Frequency

2. Growth regime:

It is generally believed that best electrical properties of the devices are obtained when the i- layers (base layers) are deposited at the interface of a-Si and nc-Si interface or so called "near-the-dege"[24]. It has been seen that devices which are deposited with larger grains have shown deterioration not only in current density but also in FF and efficiency. There can be several possible reasons like:

1. more efficient contamination in the 'grains' (as opposed to the 'grain boundaries')
2. Insufficient hydrogen passivation of defects along 'grain boundaries' (loss of H coverage if grains are deposited at higher temperature)
3. Unidentified deterioration of carrier transport in the film growth direction
4. Poor interface compatibility or higher density of p/i interface defects or something else?

3. Effect of impurities:

Nanocrystalline Silicon growth is very sensitive to the impurities and oxygen has been the main impurity affecting the material properties of the solar cells and films. It has been reported that oxygen present in the grain boundaries in electrically active and behaves as a donor state[25]. These accumulated donors at grain boundaries can cause a shunt leakage along the columnar structure which leads to lower open-circuit voltage Voc and lower Fill Factor FF. While Boron from TMB is used to compensate for the oxygen, extra boron is know to form a catalytic reaction with H_2 forming the B-H bonds and reducing the atomic H at the growth surface and hence deteriorating the crystallinity. This catalytic effect also leads to increase in the growth rate.

4. Effect of temperature:

The low temperature deposition can be preferential in terms of crystallinity and defects created as shown by Kondo[21]. Figure [2.11 shows that higher value of crystallinity is

obtained for temperatures around 200C, while it decreases on either side of it. Also shown in Figure [2.12] is that carrier density increases significantly after 200C which can be attributed to oxygen which acts as donor atoms.

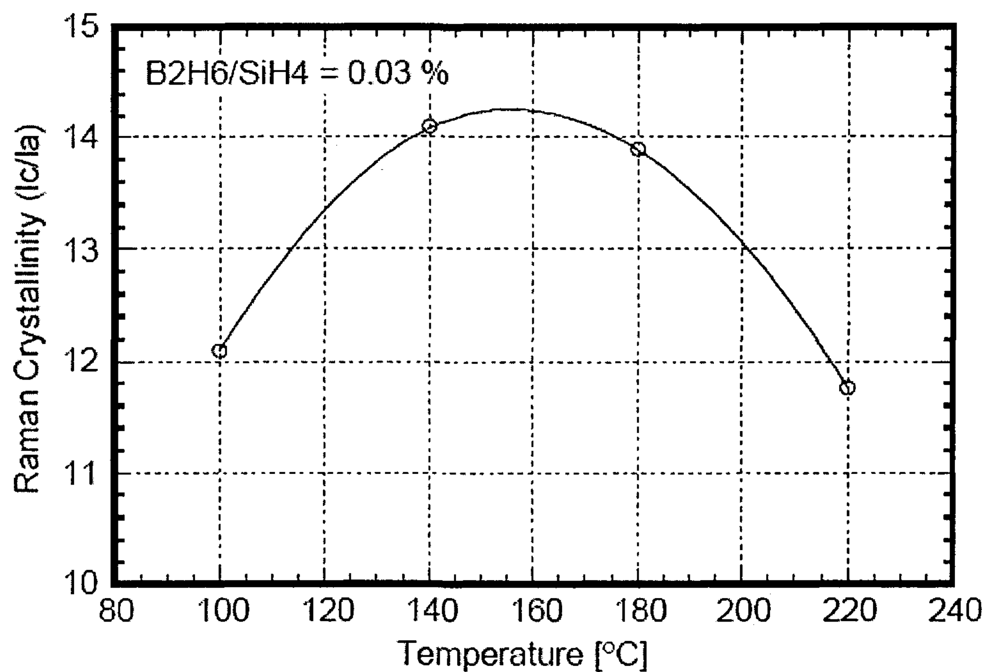

Figure [2.11]: Crystallinity vs. deposition temperature[21]

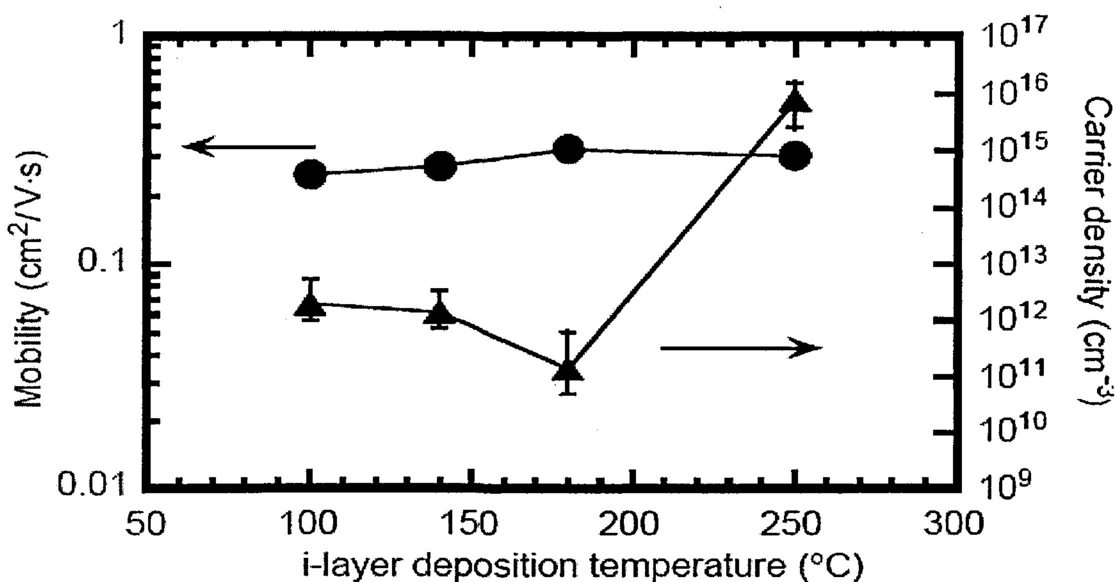

Figure [2.12]: Mobility and carrier density vs. deposition temperature

nc-Si: H as a material is very sensitive to the impurities. As it has been found that undoped nanocrystalline shows n type behavior because of the electrically active oxygen present in the grain boundaries. These accumulated donors at GB's leads to shunt leakage along the columnar structure resulting in lower Voc and FF. Decrease in the oxygen can be achieved using three techniques

1) Micro doping: In this effects of oxygen can be compensated by carefully doping the material with TMB.
2) As shown, decreasing the temperature from 250C to 180C for deposition decreases the carrier density by 4 orders.
3) Using Gas Purifier to clean the feed gases to very high purity.

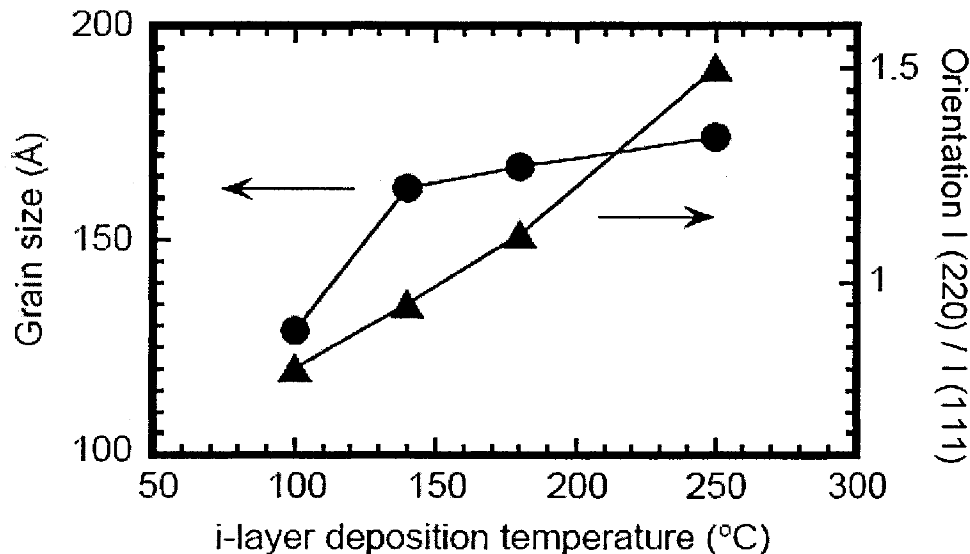

Figure [2.13]: Grain Size Vs. Deposition temperature[21]

The effect of temperature on the grain size has been shown above.

5. High efficiency devices:

Some of the high efficiency nanocrystalline n-i-p devices reported in the literature is by Yamamoto at Kaneka[27] although in this lot of efficient light trapping techniques like light trapping layers and back reflectors have been used.

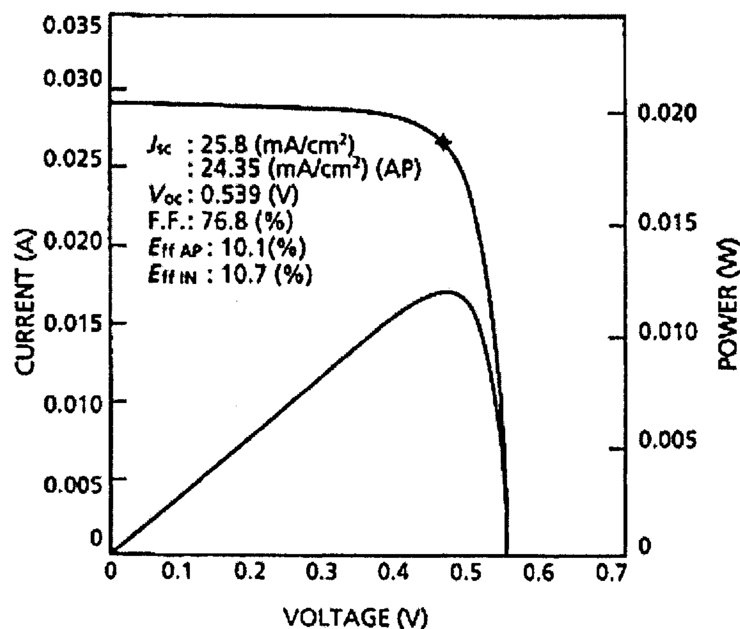

Figure [2.14]: Highest efficiency single junction microcrystalline silicon solar cell

An extensive research has been done by various groups most of which has been concentrated on the determining the electronic propertied in the films while little systematic work has been done on determining the material properties of devices since films are grown on different substrates and may lead to different material properties depending upon substrate. While the research has involved mostly around the growth mechanism, the requirement to understand the basic fundamental behavior of these devices and their electrical properties is still missing. This has been the motivation towards doing this research to understand how the basic electrical characteristics as well as doping and defects affect the device properties.

CHAPTER 3

MATERIAL GROWTH AND CHARACTERIZATION

1. Sample preparation:

Since the bandgap of nanocrystalline silicon much like crystalline silicon is indirect bandgap hence solar cell would need sufficient thickness of i- layer to have substantial absorption. It has been found that the diffusion length of electrons and holes in nc-Si: H is around 1 μm and is insufficient to ensure satisfactory collection in devices that are a few μm thick. So, drift-assisted collection of the carriers becomes important, and hence needs an intrinsic layer as photovoltaically active layer.

Devices:

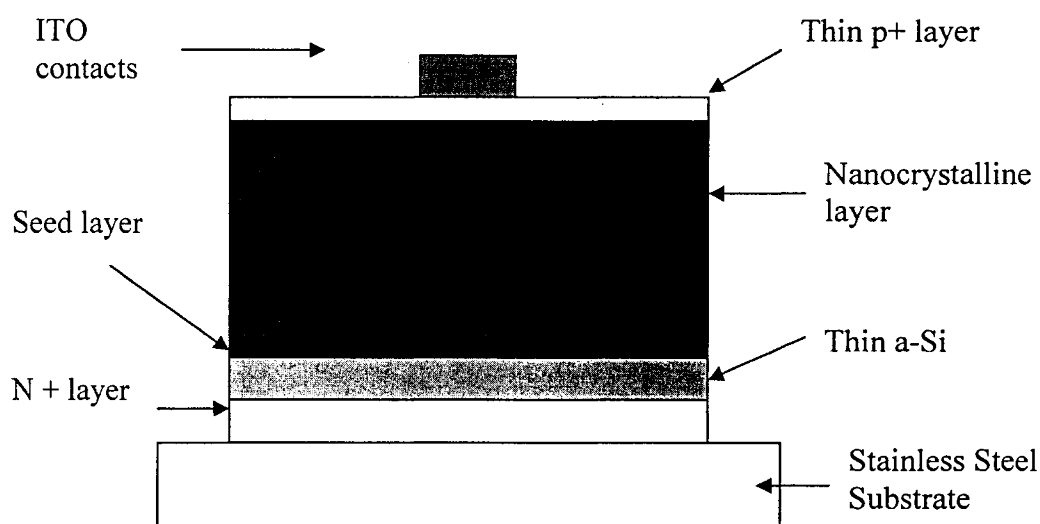

Figure [3.1]: p^+-n- n^+ device

The diagnostic devices we have studied are of the p^+-n-n^+ type as shown in Fig [3.1], with the n+ layer deposited first on a polished stainless steel substrate. The substrate is cleaned with the standard cleaning procedure of methanol and ultrasonic clean. The doped layers p^+ and n^+ are deposited using the ECR process by adding dopant gases of diborane and phosphine accordingly. Series of n+ are deposited and saved in methanol so the

reproducibility of the samples can be maintained and influence of impurities from the reactor walls with different runs can be minimized. The n^+ is then etched in Buffered Oxide Etch (BOE) solution and cleaned in DI water and methanol before being loaded into VHF reactor. The undoped base layer is deposited using a VHF diode process at 45 MHz in separate reactor to prevent cross-contamination between layers. The layers are found to be n-type. Usually a 45 min dummy is done, once the n+ is loaded followed by four hours of baking of the reactor walls to take the moisture and oxygen out of the walls. This generally brings the pressure of the chamber down by the order of a magnitude (from 10^{-6} to higher orders of 10^{-8} torr) leading to less oxygen in the system during the deposition and hence less doping in the base layer.

This undoped base layer is deposited in two stages, a nucleation stage where a hydrogen/silane ratio of 20:1 is used, and the main stage where the ratio is graded with time and reduced to 12:1 to 14:1. We have found out that once the seed layers has been deposited and the nanocrystalline layers begins to deposit, even low dilution ratio of hydrogen/silane of 12:1 can be used to increase the growth rate and also vary the grain sizes and the way it forms interface with the p^+ layer. The band diagram is shown in the Figure [3.2]. The i-layer in lot of recent devices is followed by a very thin a-Si cap layer which influences the Voc of the device. This is followed by p^+ layer which is very thin nc-Si layer and a-(Si C): H as the top layer.

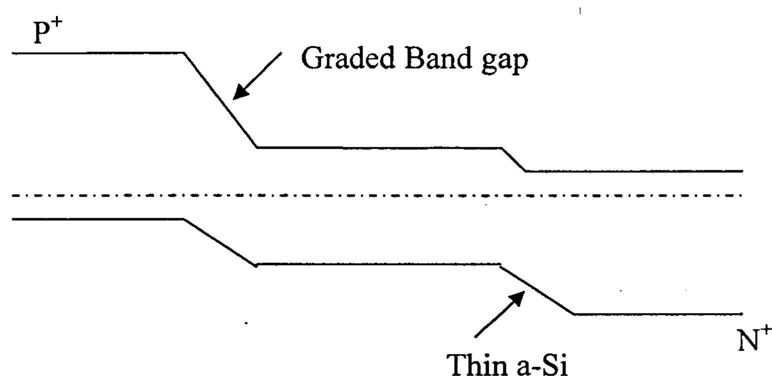

Figure [3.2]: Band Diagram of the device

The purpose of the a-Si layer is to prevent the oxidation of the top surface of nc-Si: H layer but as will be shown later it also helps in open circuit voltage. If it is too thick or if too high a bandgap is used for a-(Si C): H, inflection points occur in the I-V curve.

The top contact is transparent, conducting ITO deposited in a sputtering chamber with ITO target, done under high vacuum and Argon + O_2 environment. The deposition of the ITO is done for 2.5 min after a 2 min conditioning layer using a 20W power. The devices are later annealed at 175 C for 15 minutes to make sure we have good contact of ITO with the top layer of the device. It has also been found out that depositing 1000A of Aluminum over the ITO and driving a forward current through the contacts for few minutes brought the series resistance of the device considerably and helped in getting better FF (Fill Factor) for the devices.

2. VHF reactor:

The VHF reactor used for this study has been shown in the next Figure. It's a capacitively coupled reactor with the electrode as the lower plate. The n^+ was loaded in the substrate holder with the suitable mask which acted as the upper plate. Three heating rods are installed in holder to provide uniform heating along the substrate. The thermocouple is hooked up very close to the substrate to make sure that delta in actual and an indicated temperature is minimal. Special attention is given to make sure that proper grounding has been obtained so that stable and reproducible plasma's can be obtained every time.

As seen in the Figure, the outside walls of the reactor having heating tapes attached along them which were used to bake the reactor walls and bring the vacuum down by an order of magnitude. The constituent gases were flown from the Mass flow controllers after the careful calibration of the gas flows has been done. The plasma was started at higher pressures to make sure that stable plasma has been obtained, which would efficiently dissociate the gases and lead to desired deposition on the substrate.

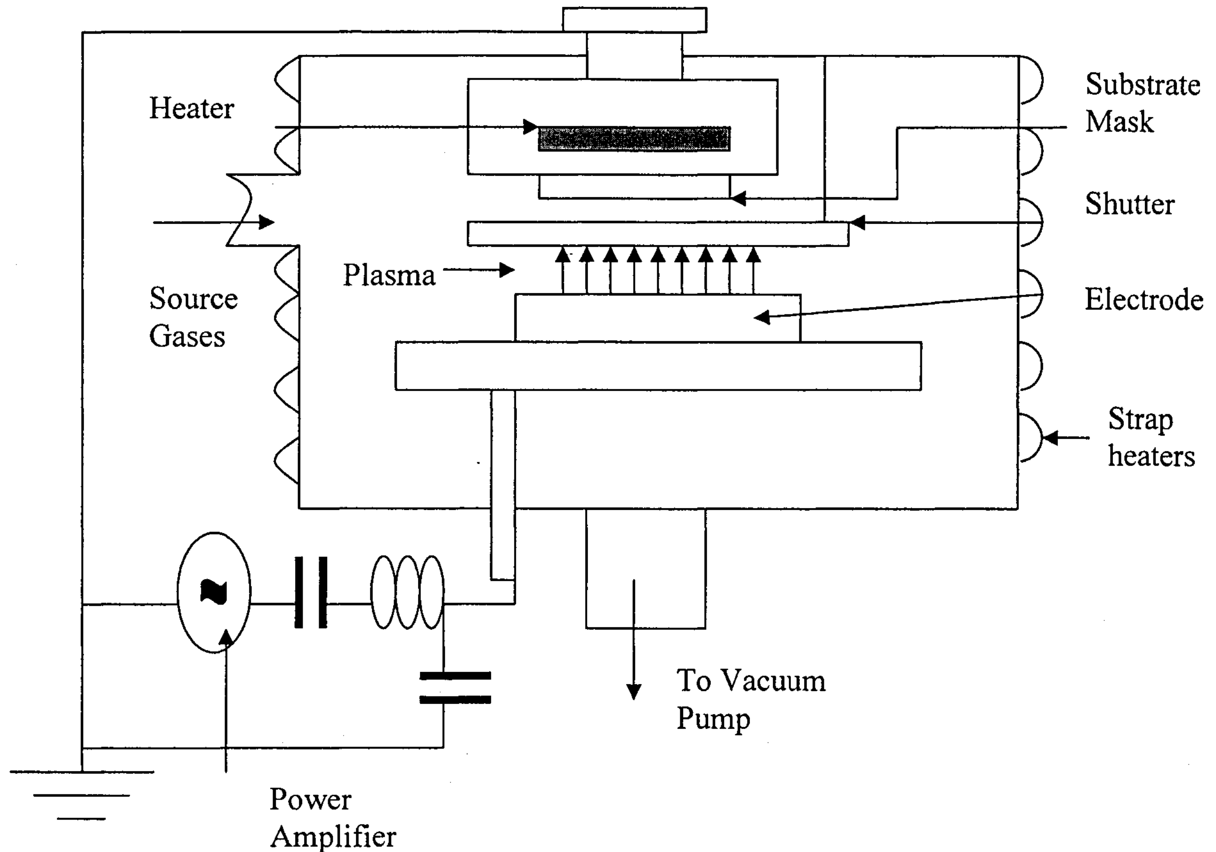

Figure [3.3]: VHF reactor used for making devices

3. Characterization techniques:

Various characterization techniques that have been used in this study have been listed and explained below:

A. Thickness using Spectrophotometer-9
B. I-V Analysis
C. Quantum Efficiency Measurements
D. Measurement of doping and defect densities
E. Measurement of diffusion length of holes
F. Structural Measurements
   1. Raman Analysis
   2. XRD Analysis

A. Thickness:

The thickness of the films is determined from the period of oscillations in the transmission versus wavelength curve in the 1000 to 2500 nm range using the spectrophotometer-9, by using the equation

$$t = \frac{i}{2n\Delta(\frac{1}{\lambda})} \qquad (3.1)$$

$$\text{where } \frac{1}{\lambda} = \frac{1}{\lambda_1} - \frac{1}{\lambda_2} \qquad (3.2)$$

where i is the number of complete cycles from $\lambda_1$to λ_2 which are the wavelengths of the i cycles. For the two adjacent maxima or minima, i =1. Figure [3.4] shows the signature transmission of devices which can be used to extract the thickness

n_l is the index of refraction and is usually a function of the wavelength used for the nc-Si: H films over the above wavelength range.

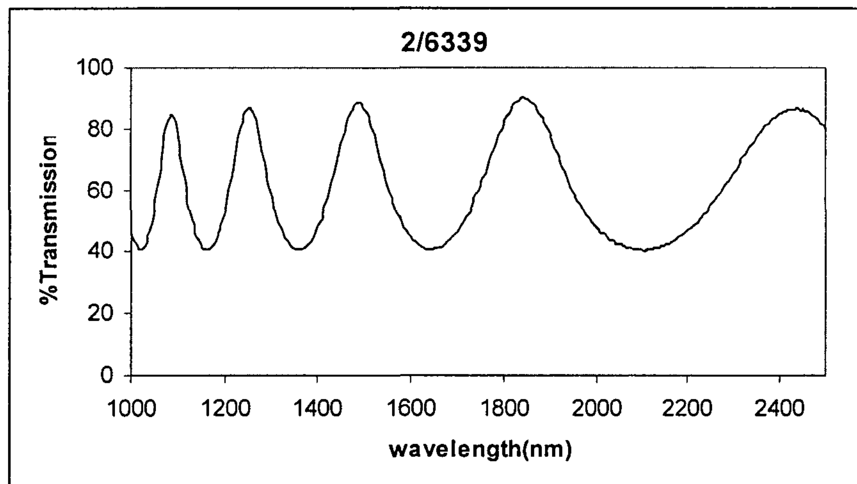

Figure [3.4]: Plot of % Transmission Vs Wavelength obtained from Lamda-9 spectrophotometer

B. IV analysis:

IV curves, under illumination are measured using an ELH lamp set up. The lamp was adjusted to 1.0 sun intensity using a calibrated Silicon solar cell for 1.5AM sun spectrum. Figure [3.5] shows a typical I-V curve for a device made using the VHF process without any special back reflector or light trapping layers. The current density is 13.5mA/cm^2, the voltage is 0.46V and the fill factor is 0.65. The n layer thickness was ~1.2 micrometer. The corresponding quantum efficiency curve is shown in Figure [3.7]

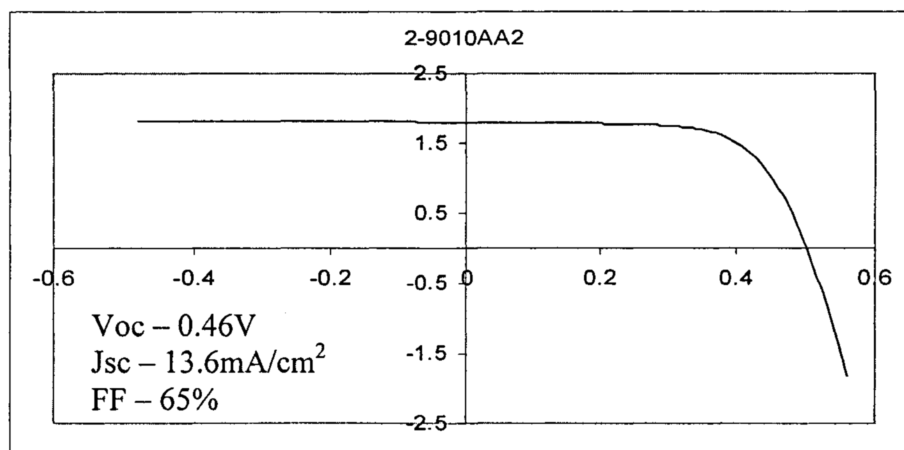

Figure [3.5]: Typical IV curve of the nc-Si

C. Quantum efficiency:

Quantum efficiency of the devices was measured using the setup as is shown in Figure [3.6]. In this setup the DC beam light of (~1Amp) shines on the sample to fix the quasi Fermi levels (and hence fix carrier life times) and the small AC light measures the photoconductivity for the sample. The ac beam superimposes on the dc beam and thus modulates the photocurrent generated in a sample by creating the additional electron-hole pairs. The change in the photocurrent produced in the sample with the change in wavelength of the ac beam from the monochrometer can be detected by a lock in amplifier with signal being amplified using a pre-amplifier.

The range of the monochrometer that we have used is from 400 nm to 900 nm where the output light is chopped by chopper modulating the photon signal to produce 13.5 Hz square wave. This reduces the noise due to ambient light and 60 Hz power lines. High pass filter of 700nm is used to get rid of the lower wavelengths and to reduce second harmonics while doing measurements above 700nm.

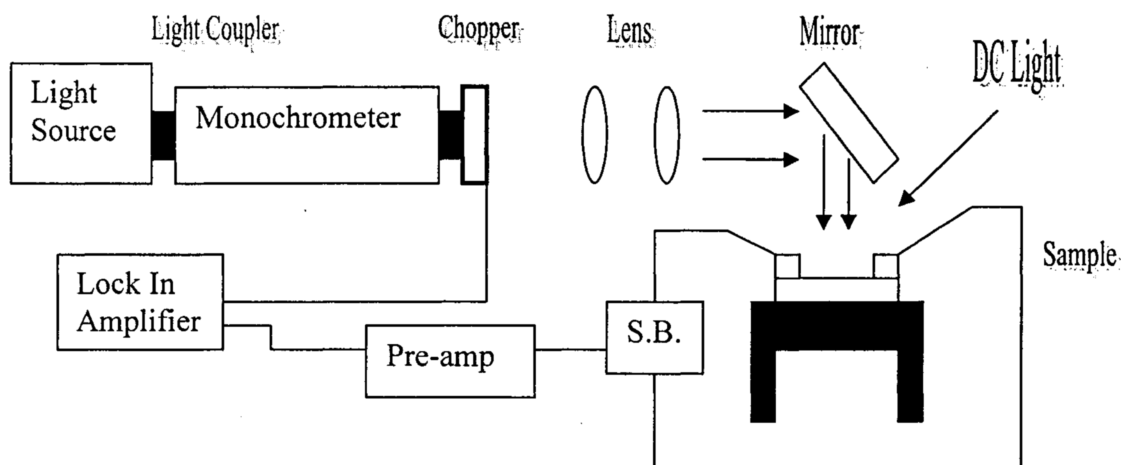

Figure [3.6]: Quantum Efficiency Set up

The measurements are made at 0 and -0.5 V. During the reverse bias, the depletion width in the i-layer increases. Since no considerable gain in the collection is obtained with increasing the depletion width, which is given by the ration of collection at zero and reverse bias, it shows the high diffusion length of the minority carriers and that most of them make it at zero bias to the depletion region.

While the relative quantum efficiencies at lower wavelengths, which correspond to higher energy and are absorbed at top layers of the device which is primarily p^+, give information about the p^+ -n interface, the QE values at 800nm and around are from the absorption in the Nanocrystalline layer. The higher the QE value at these wavelengths imply higher crystalline fraction in our films.

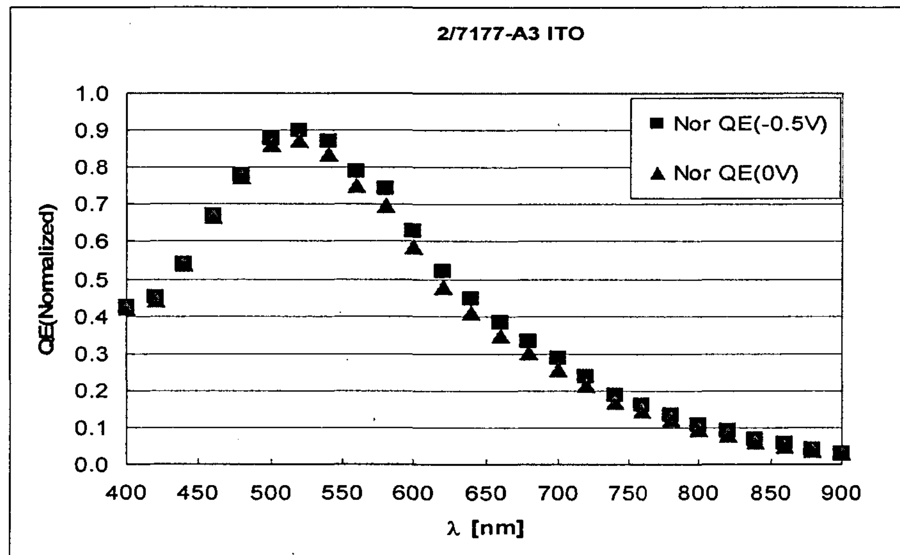

Figure [3.7] Relative Quantum Efficiency vs. voltage

D. Measurement of doping and defect densities:

C-V measurements are plotted as $1/C^2$ Vs V at different reverse bias voltages as seen in Figure [3.8] using an Agilent CV meter. The measurements are made at room temperature and using drive voltage of 100mV. The standard frequency used is 120 Hz and the measurements are done with the dark box covering the sample so that the surrounding ac-light does not influence the measurements. The instrument is calibrated every time before the measurements for open and short circuit corrections before the measurements are made. At this lower frequency we allow sufficient time for most of the carriers, even the ones in deep states, to respond to change in polarity. From the work of Kimerling[28], it is well known that if one uses a low frequency capacitance, one can estimate the total doping and defect densities by plotting the effective capacitance vs. reverse voltage, i.e. versus the thickness of the depletion layer. At low reverse voltage, one gets an estimate of doping density alone; at higher voltages, one gets the total of (doping + deep defect) densities. The slope decreases (doping increases) with voltage and then saturates, as expected from Kimerling's model. The difference between the two values of Nd_2 and Nd_1 gives the value of defect density in the material. These measurements were even used for calculating the diffusion length in the material as explained later.

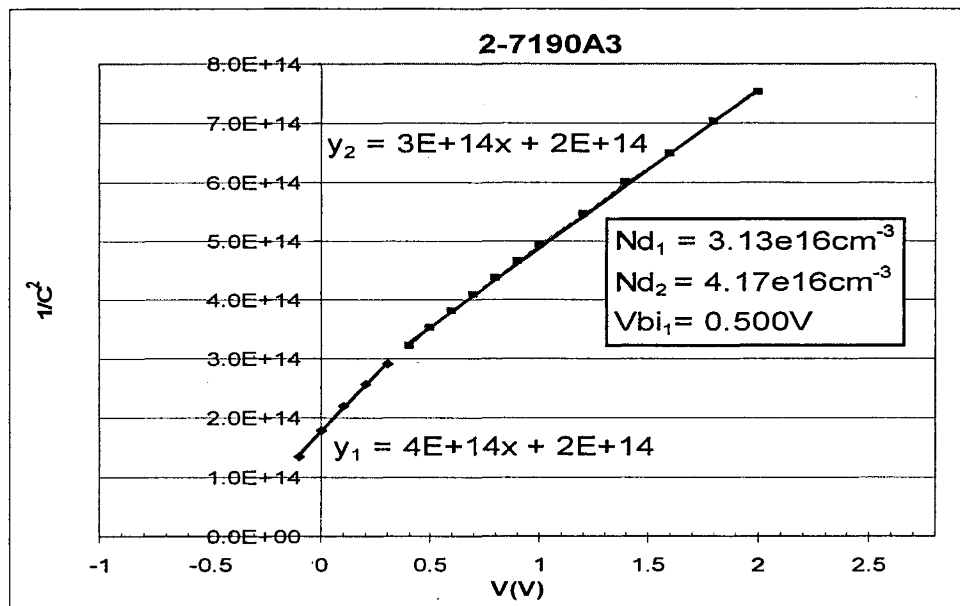

Figure [3.8]: C-V curve for device

E. Measurement of diffusion length of holes:

The diffusion length of holes was measured using relative quantum efficiency vs. reverse bias voltage techniques in combination with capacitance-voltage measurements. It is easy to show (derivation in the Appendix A) that when α Lp <<1 and t/ Lp <<1, where α is the absorption coefficient, and t the thickness of the undepleted base layer, and Lp the diffusion length,

$$QE \sim \alpha (W_d + Lp) \qquad ..... [1]$$

where, W_d is the depletion width determined from low frequency capacitance value. With varying voltage, varying depletion width can be plotted against relative QE signal, (measured at 900 nm); the intercept gives an estimate of diffusion length. Also using different values of diffusion length, theoretical QE can be calculated and matched with measured experimental QE as shown in Fig [3.9 & 3.10].

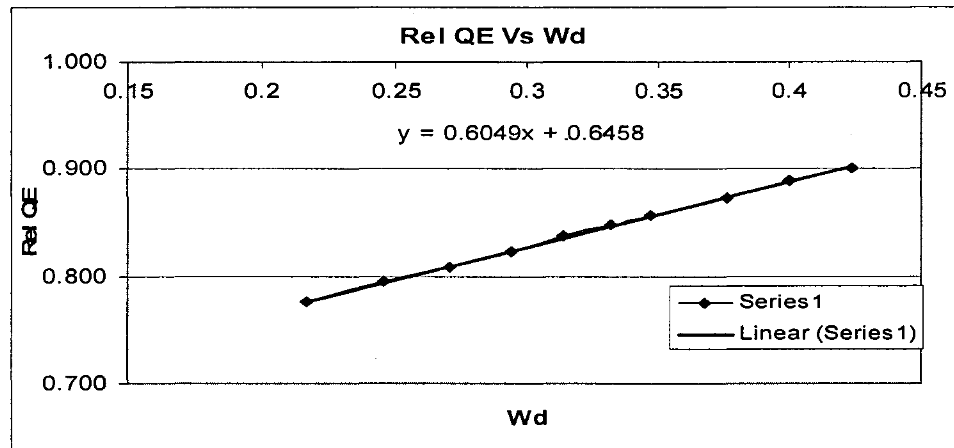

Figure [3.9]: Relative QE Vs Depletion width intercept of which gives Diffusion length

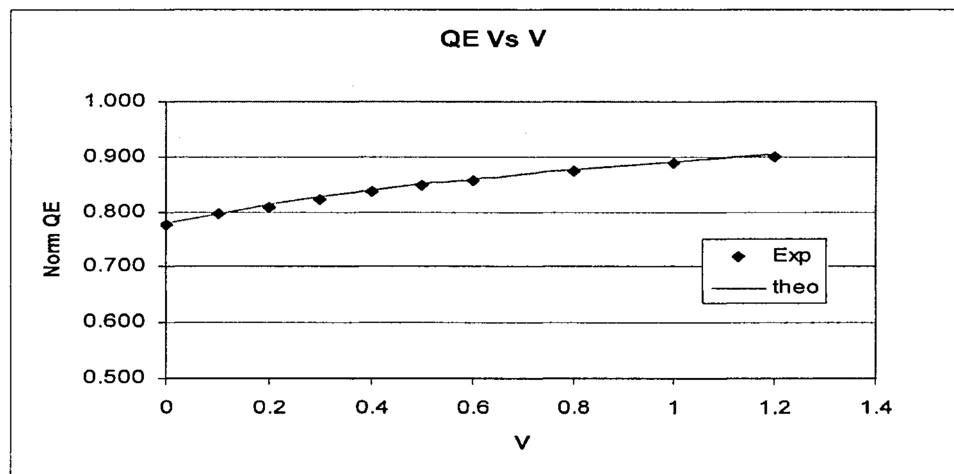

Figure [3.10]: Lp measured from the above plots to be 1.05 μm

F. Structural analysis:

1. Raman analysis:

Raman Analysis is the standard technique used in determining the amount of crystallinity in the film. Raman spectra has been obtained on some of the nanocrystalline layers that have been used in the devices, which clearly showed highly crystalline base layers, with a Raman peak ratio of about 3.8:1 or higher. The growth temperature for the base

layer was kept low, ~250 °C, so as to preserve hydrogen bonding at both grain boundaries and in the a-Si: H tissue. Use of temperatures in excess of 350 °C generally resulted in a poorer device. As seen the Raman shows the peak at 520 cm^{-1} related to crystalline fraction and a smaller peak around 480 cm^{-1} for amorphous matrix in the film. Further details on the use of Raman Spectroscopy for determining structure have been explained elsewhere[29].

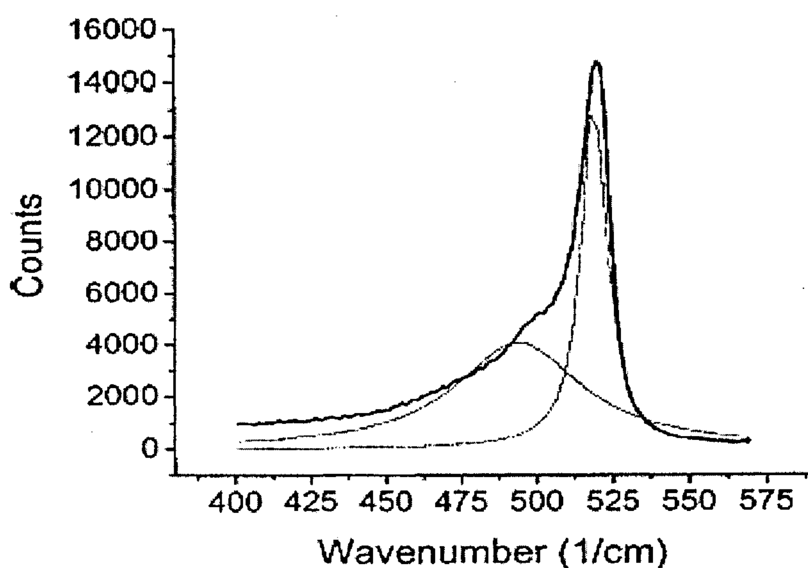

Figure [3.11]: Raman for nc-Si film[29]

2. X-ray Diffraction (XRD) analysis:

XRD relies on the dual wave/particle nature of x-rays and provides information about the structure of the crystals depending upon the diffraction pattern. As shown in the Fig [3.12] below, the peaks corresponding to different crystallographic directions have been shown[29]. When we do the VHF deposition at very low pressures, we get more of <111> oriented grains which is same as from the samples made in ECR. Some other groups have shown <220> oriented grains in the direction of growth. The big spike seen next to <220> is from Iron found in the stainless steel substrate

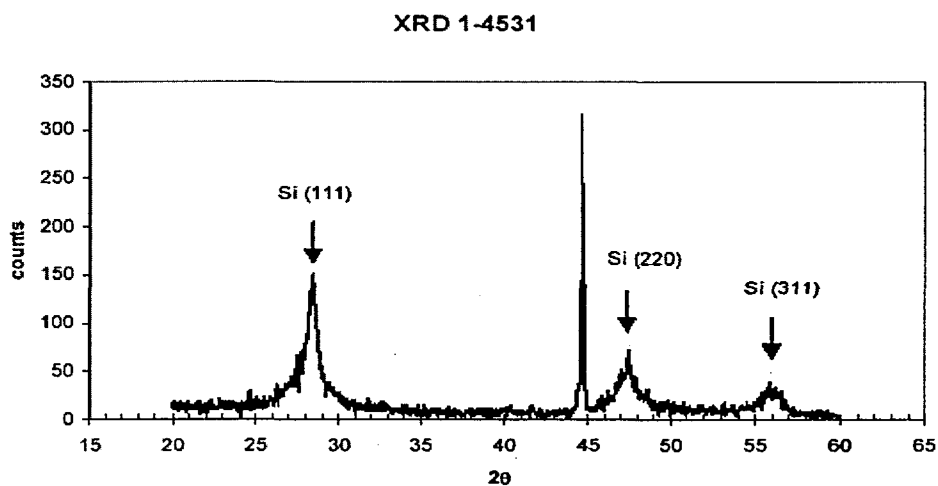

Figure [3.12]: XRD analysis for film made in VHF reactor[29]

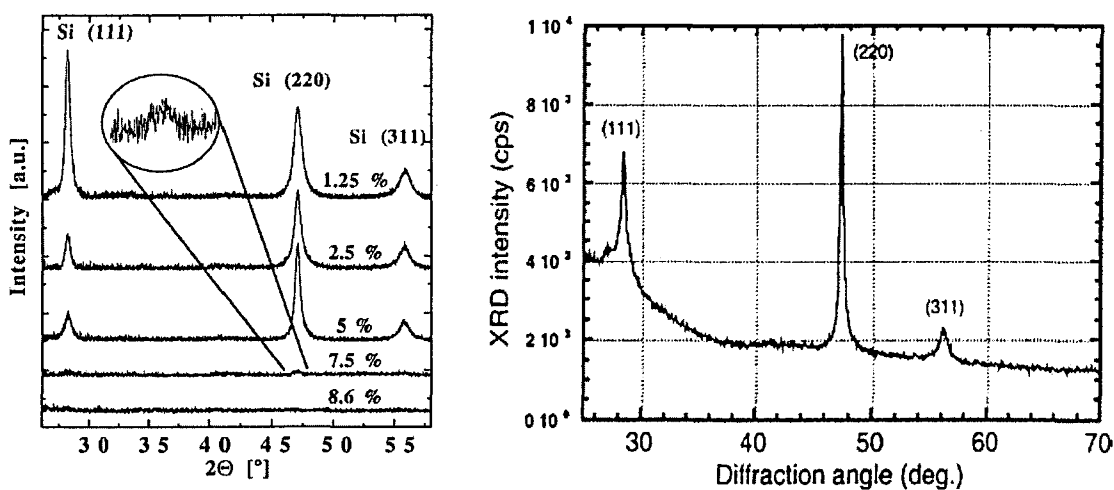

Figure [3.13]: XRD showing the variation of <111> and <220> peak with varying silane to hydrogen concentration[30] *and higher <220> peaks obtained at higher pressures*[30]

Figure [3.13][30] shows the role of hydrogen in the growth of nanocrystalline silicon. As the ratio of silane to hydrogen is decreased bigger peaks are obtained for <111> and <220> oriented grains.

CHAPTER4

RESULTS AND DISCUSSION

In this section, I discuss in detail about the systematic research done to find out the effects of various deposition parameters on the material and electrical properties of nc-Si devices. Most of the results are on p-i-n devices as described before which really turned out to be p+nn+ devices. This chapter will talk in detail about the effects of dopants (TMB and PH_3) on the electrical properties and how they affect the defects and doping in the devices along with changing the diffusion lengths. Then effects of changed in the other parameters including the effects of pressure, temperature and seed layers have been studied along with dilution of SiH_4 and H_2 will be described. Systematic work has been done here to study the effects of these parameters on device characteristics in contrast to previous work, which was on films grown on glass. Our measurements done are on actual devices.

1. Effect of ppm levels of Boron and Phosphine:

It is well known that the as grown nanocrystalline Si films are usually n type. This n type doping has been ascribed to the presence of oxygen in the films, which leads to a donor state, either within the grain, or at the grain boundaries[31]. One way to control this accidental doping is to compensate it by adding ppm levels of Boron. Boron (B) was added by using highly diluted (20 ppm in hydrogen) Trimethyl Boron gas to the silane and hydrogen mixtures. In Figure [4.1], we show the influence of adding B to the effective donor density in the material. It can be seen that the doping reduces significantly as the flow of TMB increases.

One can also change the doping by adding ppm levels of Phosphorous (P), using highly diluted phosphine (10ppm in hydrogen) to the silane, hydrogen and TMB mixtures. Here, one expects an increase in donor concentration. Figure [4.2] shows that when phosphine is added to the gas mixture, the carrier concentration increases, even when boron is present.

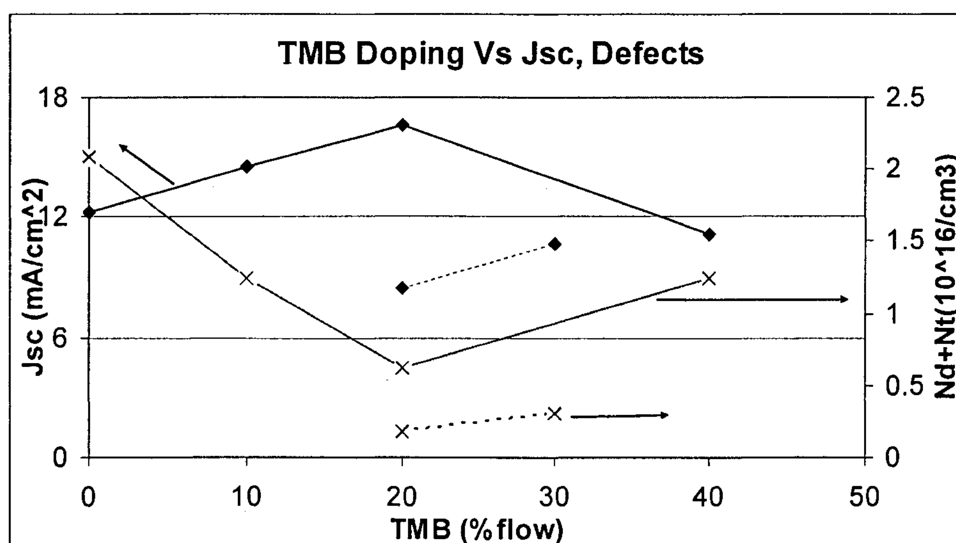

Figure [4.1]: Effect of TMB on Jsc, defects and doping

We do not know what the exact mechanism for compensation by boron (B) is. Most likely, B forms complexes with oxygen, as is the case for Czockralski grown crystalline Si, thereby removing both the donor and defect states associated with oxygen from the gap. Adding phosphine, of course, add P to the lattice, which is a donor state. Thus one expects that addition of P will increase the carrier concentration, as seen from Figure [4.2].

An interesting result of compensation is the increase in short circuit current. As the donor concentration decreases, the short circuit current increases, as seen in Figure [4.1]. At too high a concentration, the current begins to decrease again. The reason for the increase in current can be seen from the measurement of diffusion lengths in these very same samples. This result is shown in Figure [4.3], where one finds that the diffusion length of holes increases as the TMB flow increases. At too high a TMB flow, the diffusion length begins to decrease again, corresponding to a decrease in short circuit current. Thus, all the results are self consistent.

Figure [4.3] also shows the influence of adding P to the lattice on the diffusion length of holes. In agreement with the results on Czochralski crystalline Si (which usually contains significant amounts of oxygen), as the P concentration increases, the hole diffusion length decreases.

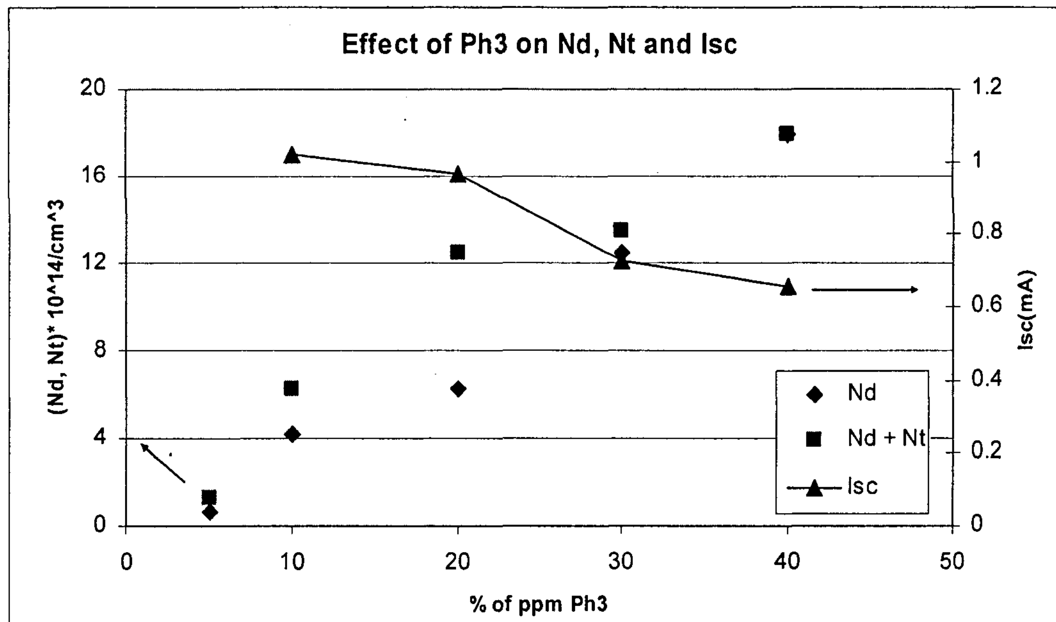

Figure [4.2]: Effect of PH_3 on doping and defects along with current density

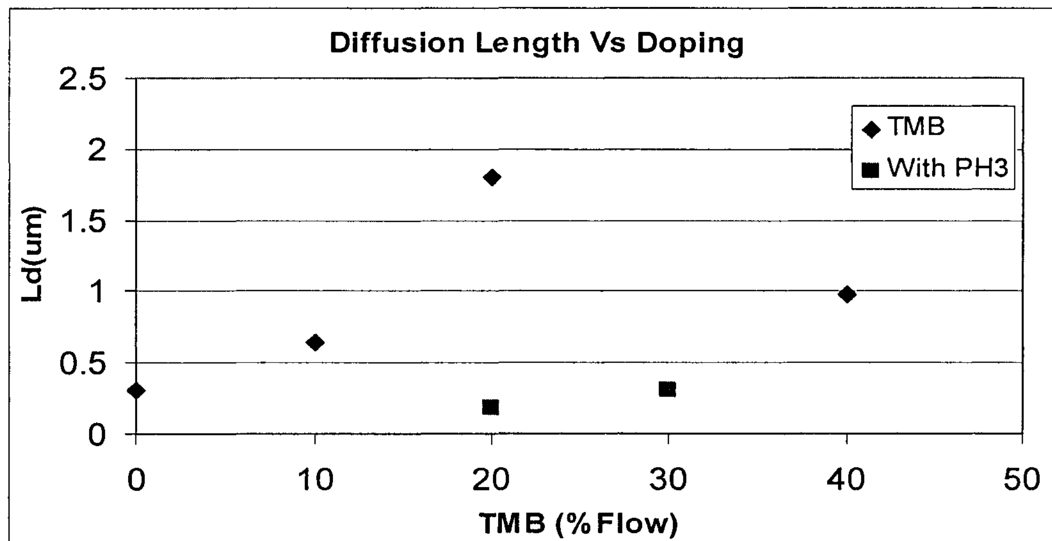

Figure [4.3]: Increasing Diffusion length with TMB compensating for O_2.

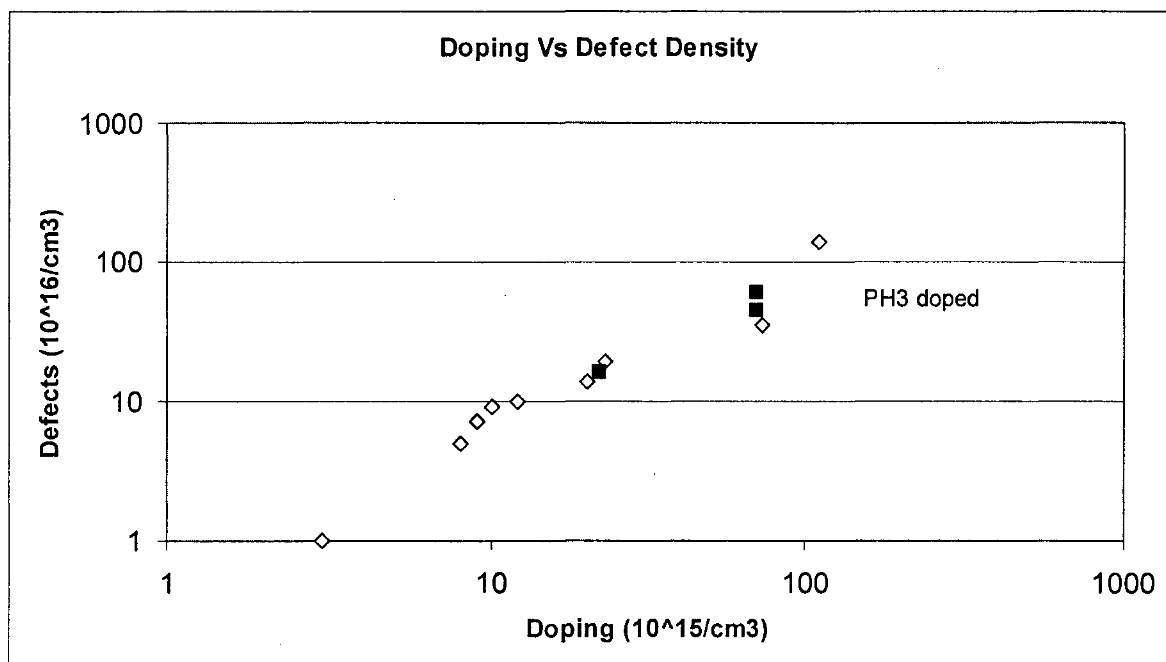

Figure [4.4] Effect of PH_3 doping[32]

2. Relationship between deep defects and net doping:

A very interesting, and unexpected, result is the influence of compensation and additional doping on the defect density, Nt. As explained earlier, variable voltage and frequency capacitance data provide us with a measurement of both shallow defect (donor) density, and deep defect (donor + deep defect) density in the base layer of the device. Figure [4.4] shows the relationship between defect density and net donor density. As explained earlier, the net donor density was changed by either adding B or P, or both. Figure [4.4] shows that as the net donor density changes, the defect density also changes with it in almost linear fashion. A similar result had been obtained using ESR measurements in films by the group at Hahn Meiner Institute[33], but at much higher donor concentration. We have been able to extend their results to carrier concentrations more typical in devices, and make the measurements in devices.

It is not clear why such a relationship should result just from doping. Perhaps, as suggested earlier, the native oxygen defects which give rise to donor states are also somehow responsible for creating deep defects in the material. The addition of B ties up some of these oxygen states, and this fact results in a reduction in deep defects. But when P is added, either additional defects are introduced through impurities in phosphine, or by phosphine forming P-B complexes, and thereby reducing the beneficial effects of B compensation. In the absence of further experiments, we cannot uniquely distinguish between these models. But I will show later on that native oxygen definitely seems to be related to the presence of donor and defect states.

3. Measurement of diffusion length of minority carriers (holes) and deep defect density:

As explained earlier, the diffusion length of holes was measured by simultaneously measuring the depletion width (using capacitance Vs Voltage) and quantum efficiency. The diffusion lengths were measured in samples with deliberately varied doping and defect densities. Appropriate conditions for measuring the diffusion lengths of the devices, as described in Chapter 3, were observed.

In Figure [4.5], I plot the relationship between the square of the diffusion length, L_d, and inverse of defect density. The basic recombination model, the Shockley-read-Hall model, for trap controlled recombination, states that square of the diffusion length should be inversely proportional to the deep defect density, assuming that the mobility is independent of defect density (and to doping, in our case). In nanocrystalline materials, since the transport is dominated by the grain boundaries, the mobility can be expected to be relatively independent of doping density and only depend strongly on the grain size. Since the grain size in our devices does not change appreciably, a result deduced from x-ray data, one expects a linear relationship between Ld^2 and 1/Nt. Figure [4.5] shows such a linear relationship, thus suggesting strongly that the SRH model is valid.

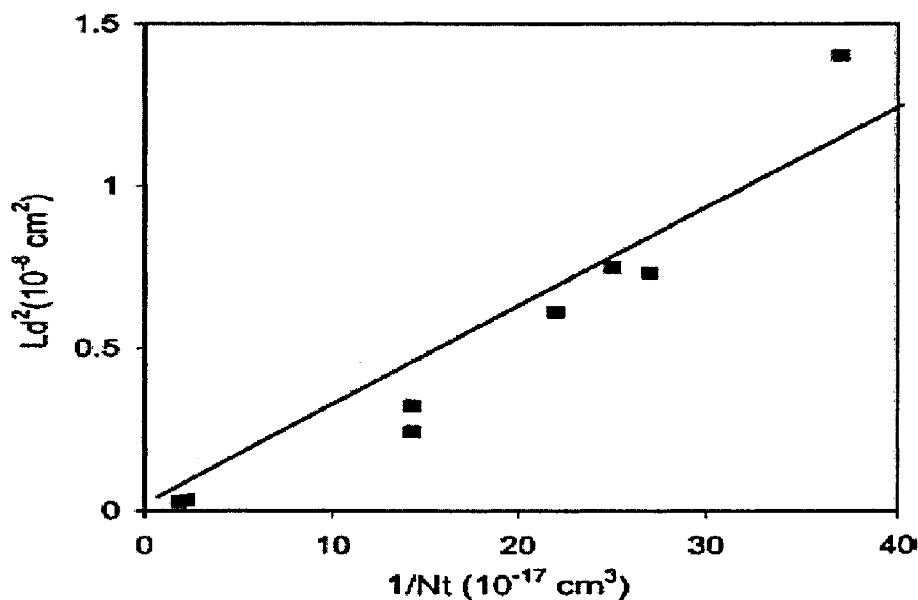

Figure [4.5] Ld^2 *vs. 1/ Nt - linear relationship*[34]

4. Measurement of location of trap levels:

One can estimate the depth of the trap level by using multi-frequency capacitance. At very high frequencies, electrons in the deep states cannot come back out in the time period of the frequency, and therefore, only the shallow traps respond, the effective depletion width is higher, and the capacitance is lower. At the lowest frequencies, electrons in all the states can respond, the effective density is higher, the depletion width is lower and the capacitance is higher. Thus, with increasing frequency, one begins to see a decrease in capacitance. This is shown in Figure [4.6].

From this figure, we see that the capacitance begins to decrease at somewhere between 400 and 1000 Hz. This sets a lower limit for the energetic location of traps. The location of the highest energy traps can be determined from the measurements done at higher frequencies on a sample whose thickness of the base layer, measured using reflection measurements, was 0.55 micrometer. As expected, at the highest measurement frequency (100 kHz), the capacitance saturates at fairly low reverse voltage.

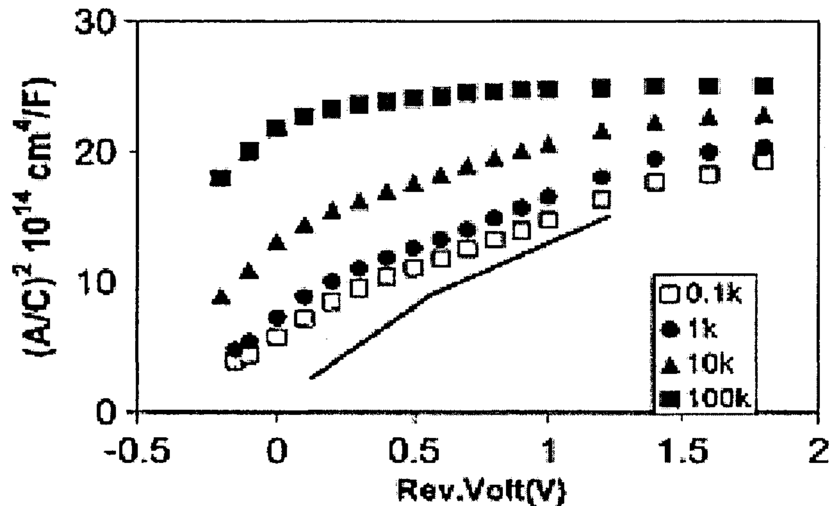

Fig [4.6] Capacitance vs. Voltage at different frequencies, Drive voltage is 100mV and measurements are done at Room Temperature [35]

Since we can measure the donor density in this sample, we can estimate at voltage where the saturation should occur. If this value of voltage agrees with the measured voltage for saturation, assuming the usual value for built-in voltages (~0.8V), then the deep states are not responding at this frequency. From Figure [4.6], the donor density was estimated at 7-8*10^{15} cm^{-3}, and the deep state density also at around 8*10^{15} cm^{-3}. Thus, if only the donors were responding, the saturation should occur at ~0.7 V, corresponding to geometrical capacitance. That is the range in which the saturation in capacitance occurs in Figure [4.6] at a measurement frequency of 100 kHz. And the measured value for capacitance also agrees very well with the geometrical capacitance corresponding to the thickness of the base n layer. Thus, we can assume that the shallowest traps correspond to a measurement frequency of ~100 kHz, and the deepest to a frequency of 400 Hz.

Now we can use the standard equation for attempt to escape frequency,

$$\nu = \nu_0 \exp[\frac{-(E_c - E_t)}{kT}] \qquad \text{.............. (4.1)}$$

to estimate the depth of the trap Et below the conduction band. The standard value for νo is ~$1*10^{11}$ sec^{-1}. Then, at 400 Hz, the trap depth is 0.5 eV, and at 100 kHz, the trap depth is 0.36 eV. Therefore, we estimate that the deep traps are in the range of 0.35 to 0.5 eV below the conduction band. Note that this value will change a little if we change the value of νo, but given the logarithmic relationship between the trap depth and νo, it will not change much. A method for measuring νo is to estimate the carrier lifetime and defect density at the same time, and then determine νo in that sample. Such measurements are being pursued by other students in the group.

5. Dark IV curves and crystallinity:

Dark I-V curves of diodes yield very valuable information; in particular, they allow one to determine the type of recombination, and to see if trap-controlled recombination dominates.

The dark current measurements for two cells are shown in Figure [4.7] and [4.8]. The cell corresponding to Figure [4.7] was made using an ECR plasma process and the one corresponding to Figure [4.8] using the VHF plasma process. The sample made with the ECR process shows an I-V curve which can be deconvoluted into two parts, one corresponding to exp (qV/2kT) and one corresponding to exp (qV/kT), as shown there. Thus, this cell follows the standard model of a diode, where the current comes from both a generation-recombination region in the depletion layer and diffusion from the bulk. But the curve in Figure [4.8] cannot be deconvoluted into two simple parts, suggesting that it is less crystalline and more amorphous. When Raman spectra were measured on these same cells, the ECR cell showed a Raman ratio of >4:1, whereas the VHF cell had a lower Raman ratio, ~3:1, thus agreeing with the I-V curves. Note also that the ECR cell had a higher mid-level defect density than the VHF cell, which of course adds to the GR current component.

Note that one can change the nature of the I-V curves in the cells made using the VHF reactor by adding to the deep level impurities, e.g. by adding phosphine. Then the generation-recombination current, the one corresponding to exp (qV/2kT) should increase, and one should be able to distinguish between two parts.

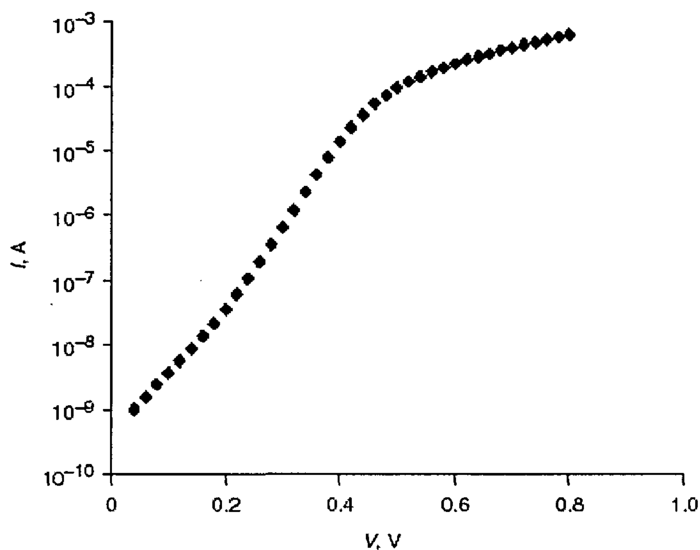

Fig [4.7] Dark IV curve from sample from ECR Reactor[29]

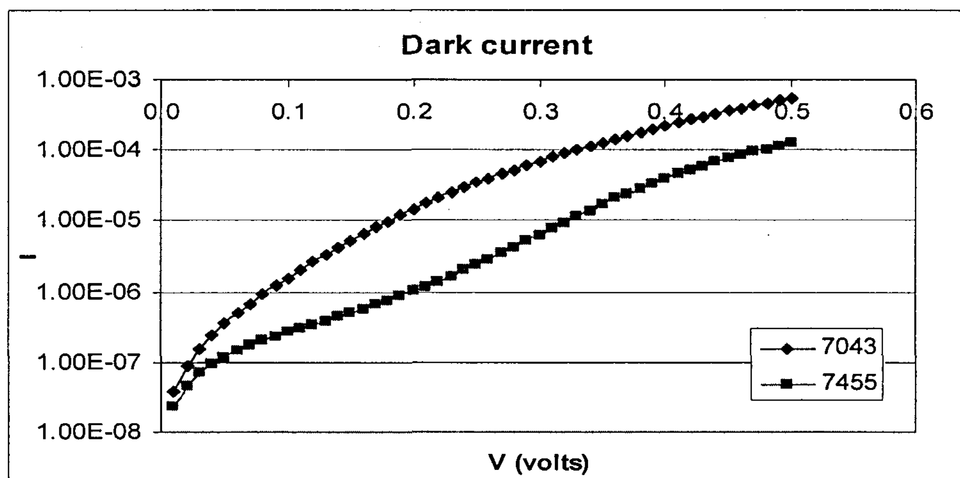

Figure [4.8]: Dark IV curve for 7043 showing distributed defects from VHF reactor

This was observed, as shown in Figure [4.9], where I show the data on dark I-V curves for a number of cells with varying PH_3 doping. As expected, s the concentration of PH3 in the gas phase increases, the curves become more 2-region like. Note also that the initial portion of I-V curve, which is the one dominated by the GR component, increases sharply as PH3 increases, as expected

6. Effect of Hydrogen dilution:

It has been known for a while that the best performance appears to be achieved when the materials has some degree of amorphous phase in it. This may be because of a number of reasons:

1. The amorphous phase may be necessary to better compensate the grain boundaries, particularly the large grain boundary.
2. The amorphous phase may prevent formation of columns and cracking if the grains become too large. It may lower the strain in the layer.

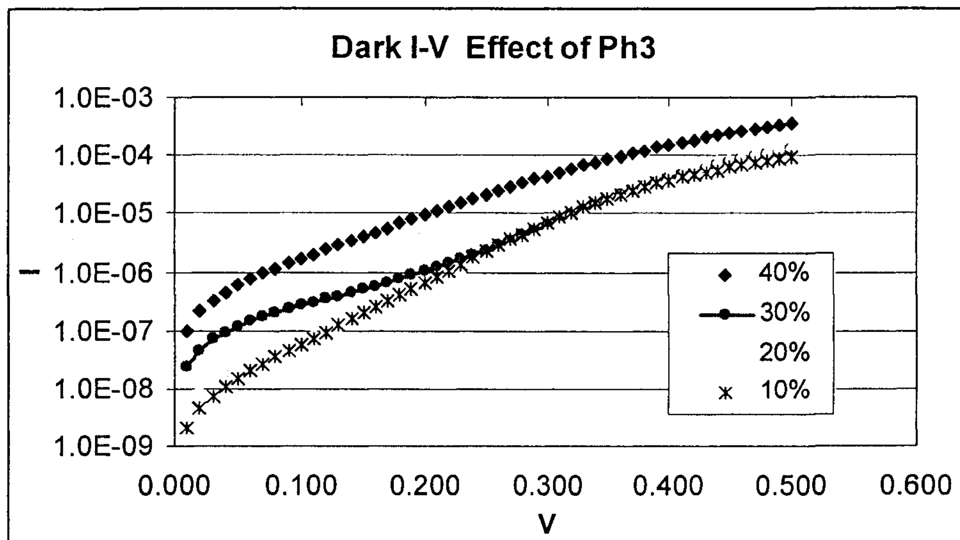

Figure [4.9] Dark IV curve of VHF deposited sample along with 2/7455 with PH_3 added

In any event, it is known that as the thickness increases, grain sizes increase and amorphous phase decreases. To maintain a more uniform amorphous phase, it was suggested by[36] that one should use H grading, such that H dilution is decreased as the thickness increases. The decreasing H concentration would serve to keep some degree of amorphous phase in the device throughout its thickness. In agreement with the previous results, we also found that both current and open circuit voltage increased as the hydrogen dilution was

reduced. See Figure [4.10] for relationship between H grading and short circuit current, and Figure [4.11] for the relationship between Voc and H grading.

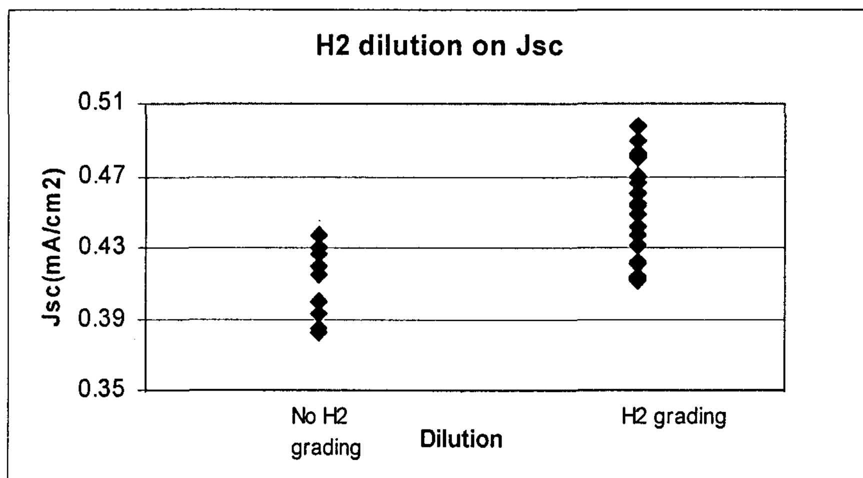

Figure [4.10]: Effect of H_2 dilution on the Jsc of the devices

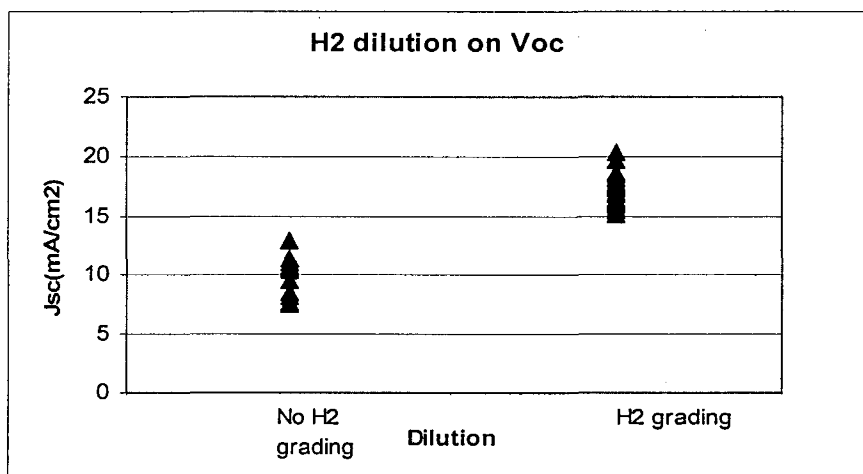

Figure [4.11]: Effect of H_2 dilution on the Voc of the devices

We also measured defect densities and diffusion lengths in devices made with and without H grading, keeping everything else constant. Figure [4.12] shows the influence of H grading on defect density and diffusion length for two samples which were otherwise

identically prepared. It is clear from this data that the diffusion length and defect density both improve as H grading is introduced

7. Use of graded ppm B doping to improve carrier collection:

Another method for improving the carrier collection is to use graded B doping. The principle of the technique is shown Figure [4.13]. By grading the effective n-type doping level with graded ppm compensation with B, one can induce a built-in field to assist the transport of holes towards the p+ junction layer

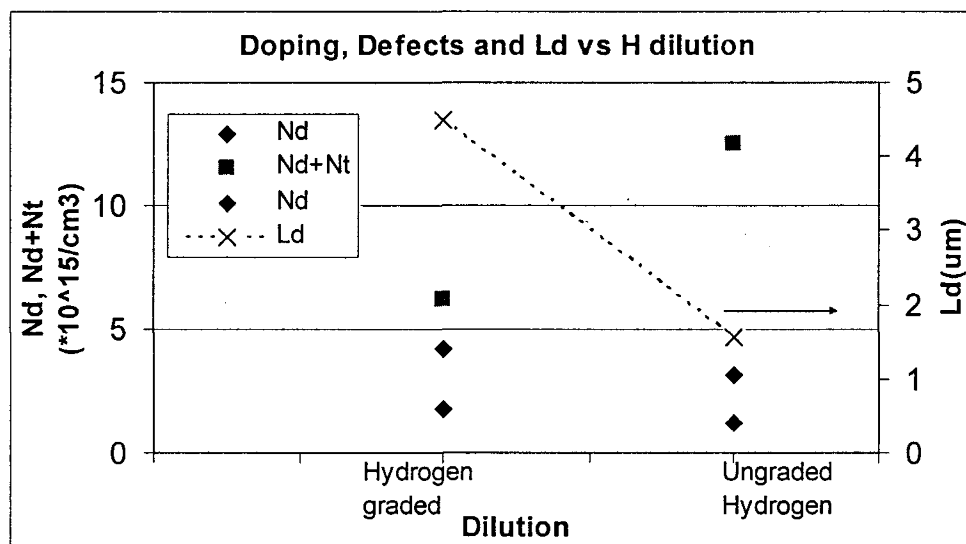

Figure [4.12]: Effect showing higher defects and lower Ld with no graded H_2 *devices*

Therefore, it should result in higher currents and higher effective diffusion lengths. The higher diffusion length should show up immediately in QE curves, and also show up as higher collection for 800 nm photons in very thick layers. This was indeed observed. Figure [4.14], I show the QE vs. reverse bias curve for a sample with graded ppm B doping, and the fit of the data to the model shows an effective diffusion length of >10 micrometer! Of course, now the transport is no longer controlled by diffusion but by drift as a result of the internal doping-induced field. The corresponding device I-V curve is shown in Figure [4.15],

showing excellent current densities (20 mA/cm^2). The increase in QE at 800 nm for a ppm B graded Vs an ungraded cell is shown Figure [4.16].

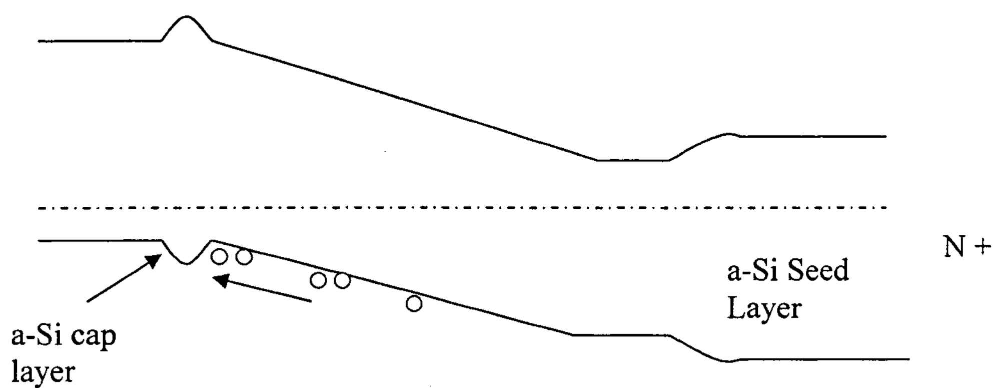

Figure [4.13]: B grading leads to higher electric field assisting hole transport

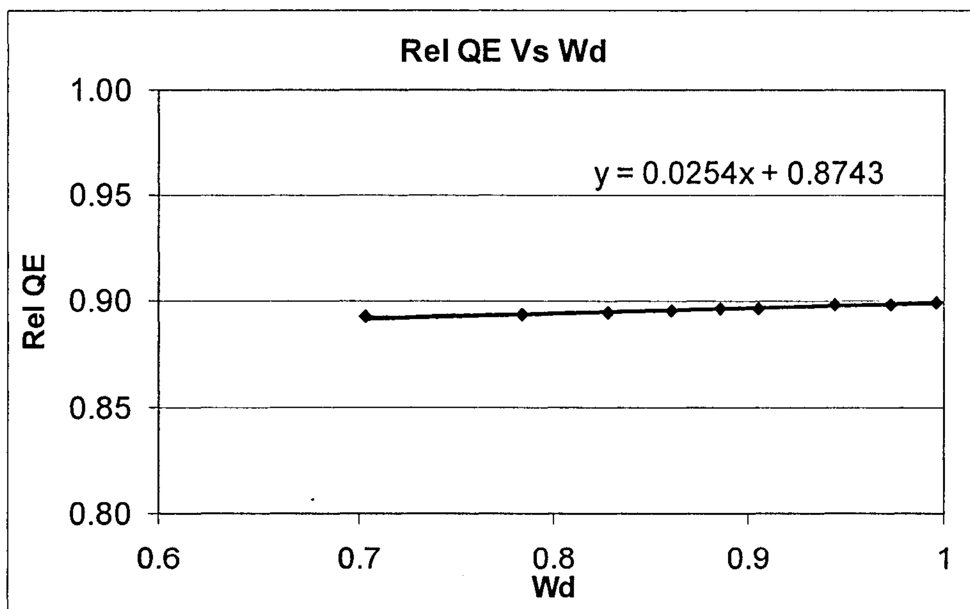

Figure [4.14]: Relative QE Vs Wd showing high Ld.

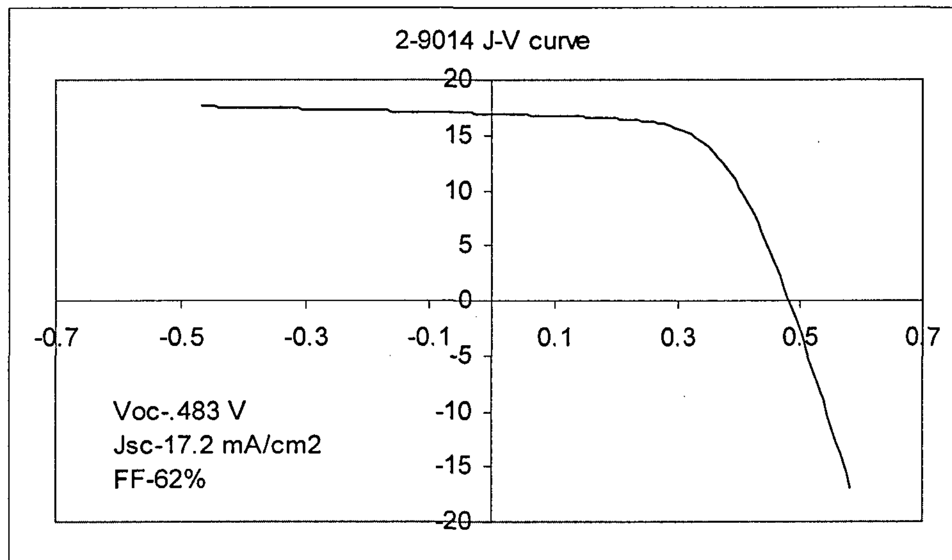

Figure [4.15] IV curve for B graded sample

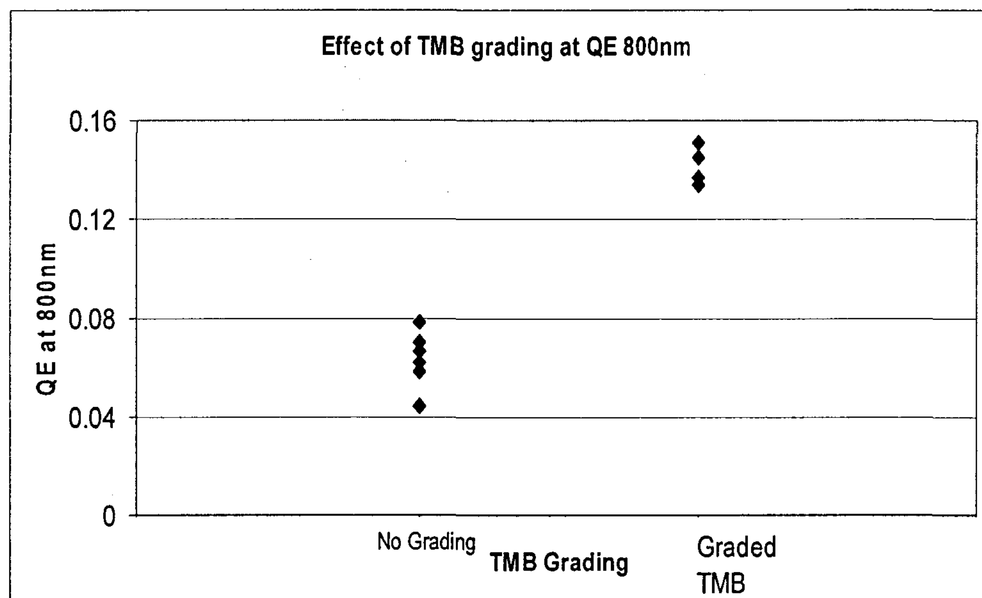

Figure [4.16]: Effect of TMB on QE at 800nm

Note that this is a new technique that we have introduced to improve the performance of nc Si: H cells. It may be very beneficial when one starts working on other materials such as nc-(Si, Ge): H and nc-(Ge, C): H cells which may not have as good properties as nc Si: H.

8. Improving voltage by the use of an interfacial capping or buffer layer between the p and the n layers:

Recombination at p+n junction interface is known to lead to reductions in open-circuit voltages in c-Si cells. To overcome such recombination, Sanyo introduced the concept of a hetero-interface, where one uses a thin amorphous Si layer followed by a p+ a-Si: H layer to make high efficiency crystalline Si solar cells[37]. The amorphous layer seems to passivate the interface, reducing recombination at that interface. We decided to see if such an interface can improve our devices, particularly voltage]. The corresponding improvement in open circuit voltages is shown in Figure [4.17], which shows that the open circuit voltages are uniformly higher when the cap or buffer layer is introduced.

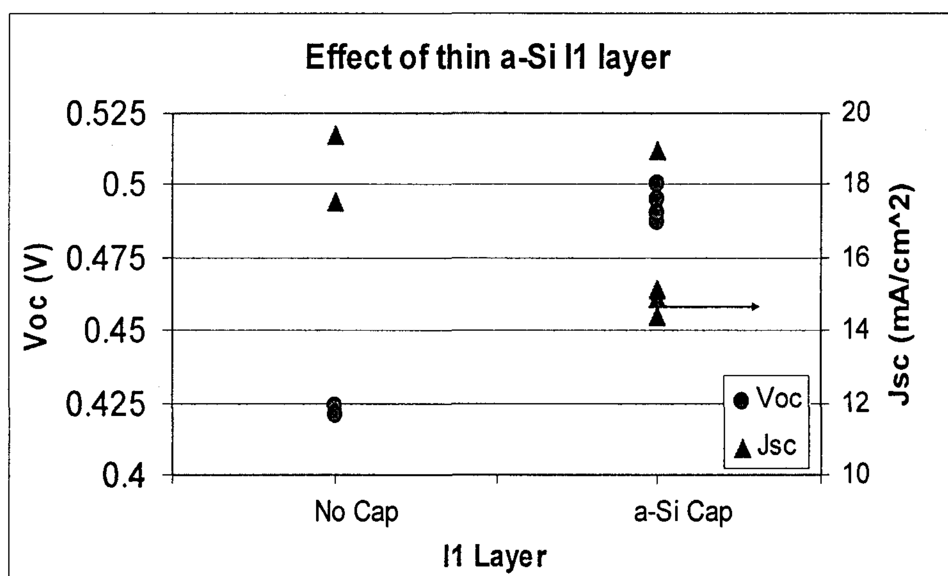

Figure [4.17]: Thin a-Si buffer layer helped in increasing the Voc.

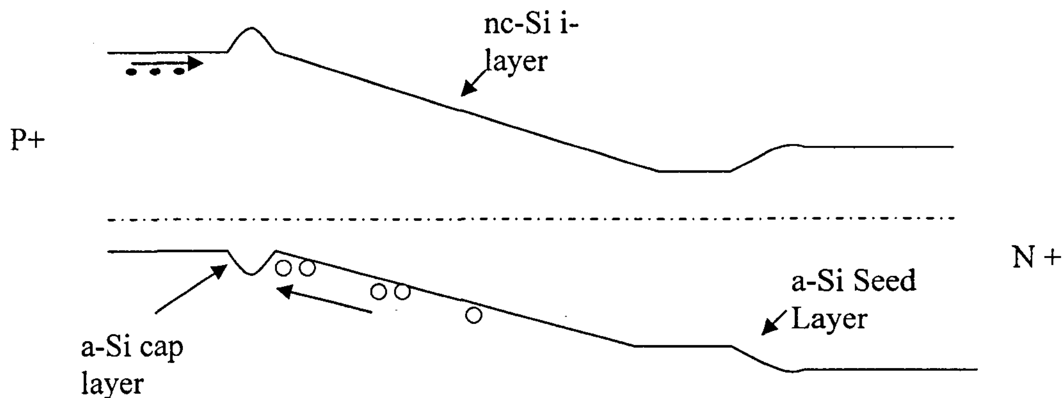

Figure [4.18]: Band diagram of device with thicker a-Si cap layer

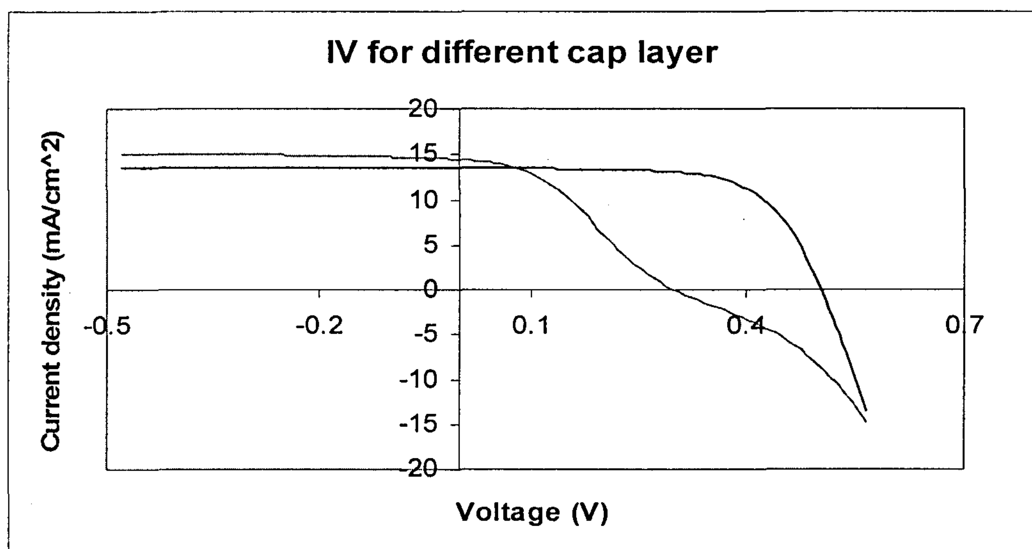

Figure [4.19] IV curve of a device showing the kink

Note that one can go too far. From Figure [4.18], we can see that adding the a-Si: H layer introduces a notch in the valence band. The notch has to be thin enough for holes to tunnel through; otherwise, hole transport would be impeded. The influence of too thick an interfacial layer is shown in Figure [4.19], where I show two I-V curves, one where the interfacial layer was thin (~10 nm), and the next where we doubled the thickness of the layer.

The second I-V curve shows a distinct inflexion point, which has been ascribed previously in a-Si: H cells to the presence of a notch in the valence band.

9. Improving fill factors by reducing series resistance:

Series resistance in the diodes is a major problem. Excessive series resistance leads to IR loss, which translates directly into a loss in fill factor of the device. Typical resistance in our devices was of the order of 50 ohms for a 0.125 cm^2 area, or about 6.25 ohm-cm^2. There are several different conditions that can lead to excessive series resistance. Among these are:

A. Resistance of ITO layer:

The top ITO layer has a sheet resistance of 15-20 ohms/sq. If only a thin probe contact is used, then current collection from the entire dot can be a problem. To reduce this resistance, the easiest method is to introduce a central metal (Aluminum) buss-bar to collect the current. Then the current collection distances are reduced and one can also probe the Al bar. Clearly light transmission is also reduced, but since we are studying fundamental material properties, and not the absolute efficiency, this is not a problem for our case.

B. The ITO/p+ interface:

In particular, since the p+ layer is thin (in order to allow for maximum light transmission into the higher quality base layer), and it is deposited at low temperatures ~ 180 C (to prevent catalytic decomposition of silane by diborane at higher temperatures), the p+ layer may oxidize, particularly during the ITO deposition, which involves energetic oxygen ions present in the plasma. This oxide layer can create problems with series resistance.

To overcome both these problems, we used a central Al buss-bar on the ITO contact (See Figure [4.20], and then annealed the contact at 175 C in air for an hour. Then, a large current (~50 mA>> solar current which is ~ 2 mA) was passed thorough the diode for 1 min by forward biasing it under light. The purpose of the thermal and the electrical anneal cycle was to punch through any thin silicon oxide layer. When this was done, the series resistance reduced in every case. In our best diodes, it was of the order of ~3.3 ohm-cm^2. Corresponding to this decrease in resistance, the fill factor in the device increased to 69%,

from the previous 60% range. See Figure [4.21]. Thus, by using this technique, we were able to produce devices with the fill factors which are in the range of the best values achieved (~70%), whereas previously, our fill factors were considerably lower. A high fill factor is a measure of how well current is being collected, and agreed with our QE and diffusion length data.

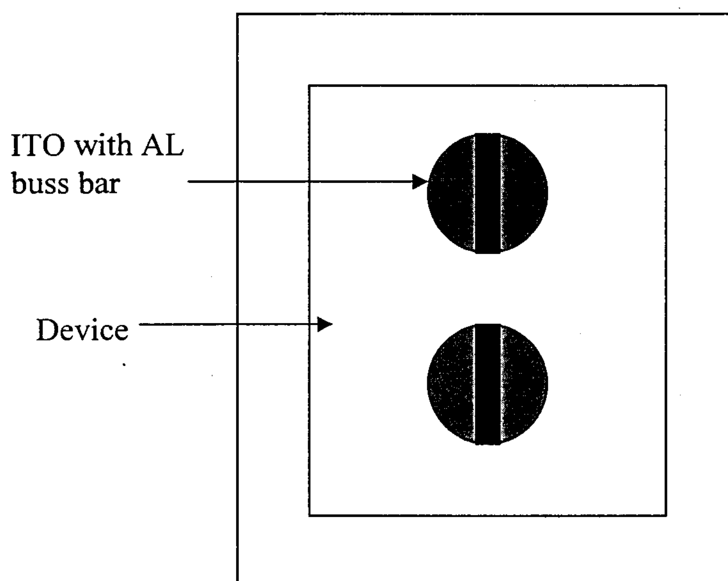

Figure [4.20]: Device with Al buss-bar over the ITO Contacts

10. Influence of seed layers on crystallinity and device performance:

It is well knows that there is a transition region between amorphous and crystalline layers when growing the nanocrystalline materials. The transition region depends upon the hydrogen/silane ratio. The higher the dilution, smaller is the thickness of the transition layer. Therefore, to speed up the transition, often a seed layer is introduced at the start of the growth, made with very high H dilution.

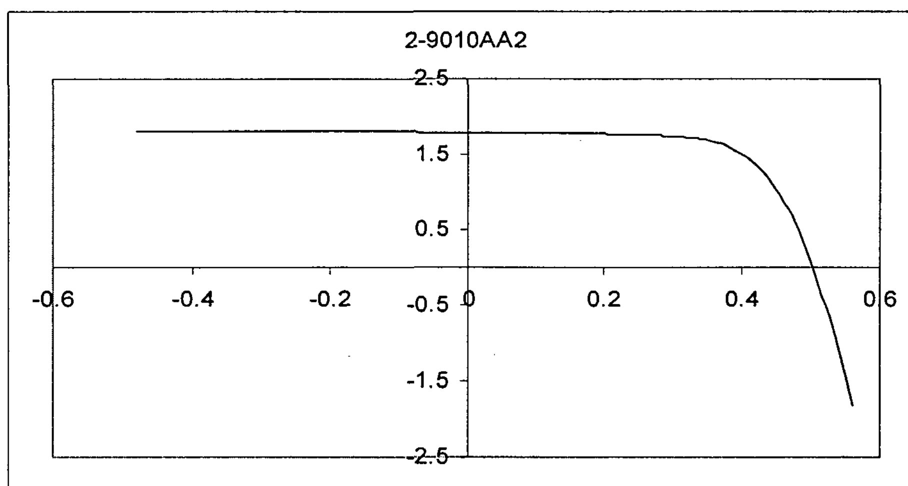

Figure [4.21]: IV curve showing 70% FF and Series resistance of 27 Ω

To study the influence of the seed layer on the device performance, a number of devices were made with and without seed layers. In particular, since the crystallinity should be improved with a seed layer, it should lead to less amorphous phase in the device, and therefore, a smaller voltage, but higher quantum efficiency at 800 nm, corresponding to higher absorption. Two devices were made with and two without the seed layer.

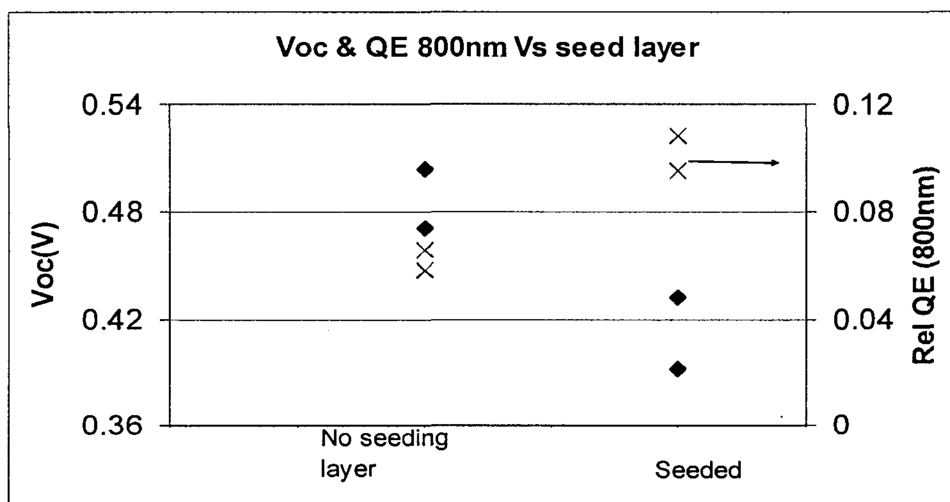

Figure [4.22]: Effect of seed layer on Voc and QE at 800nm.

The data for open circuit voltage and QE at 800 nm are shown for this twin set of devices in Figure [4.22]. It is very clear from this figure that having a seed layer leads to simultaneous lowering of voltage and increase in 800 nm QE, as expected.

11. Controlling crystallinity and device properties by dilution with Helium (HE):

The use of HE gas in the plasma offers another method for controlling crystallinity, and therefore device properties. HE is a more massive ion than H. Therefore, it should be more effective at transferring momentum to the growing lattice, and may improve crystallinity up to a point. Indeed, in companion work by my colleague, Nanlin Wang, he showed that chemical annealing with HE could transfer an amorphous film into a nanocrystalline film[38]. To explore the possibility offered by HE for control of crystallinity, a number of devices were made with varying flows of HE. Figure [4.23] shows the data on open circuit voltage and QE at 800 nm, both indicators of the degree of crystallinity. The x axis represents the % flow from the flow controller. Initially, the material does become more crystalline, as indicated by a decreasing voltage, and increasing QE at 800 nm. But at higher flows, the voltage begins to increase and the QE begins to decrease, indicting a more amorphous structure setting in. In Figure [4.24], we show the data for diffusion lengths in these same devices, and at first the hole diffusion length increases, and then, beyond 15% flow, abruptly decreases, the decrease being characteristic of a-Si: H. Thus, we have shown that it is possible to alter the device performance by controlling crystallinity with HE, offering another avenue for control.

12. Influence of deposition temperature on device properties:

It is known from previous work[39] that deposition temperature has a strong effect on device performance. There could be several reasons for this effect.

1. Crystallinity is a strong function of deposition temperature. As the temperature increases, in general, crystallinity increases, if all the other deposition parameters are kept invariant.

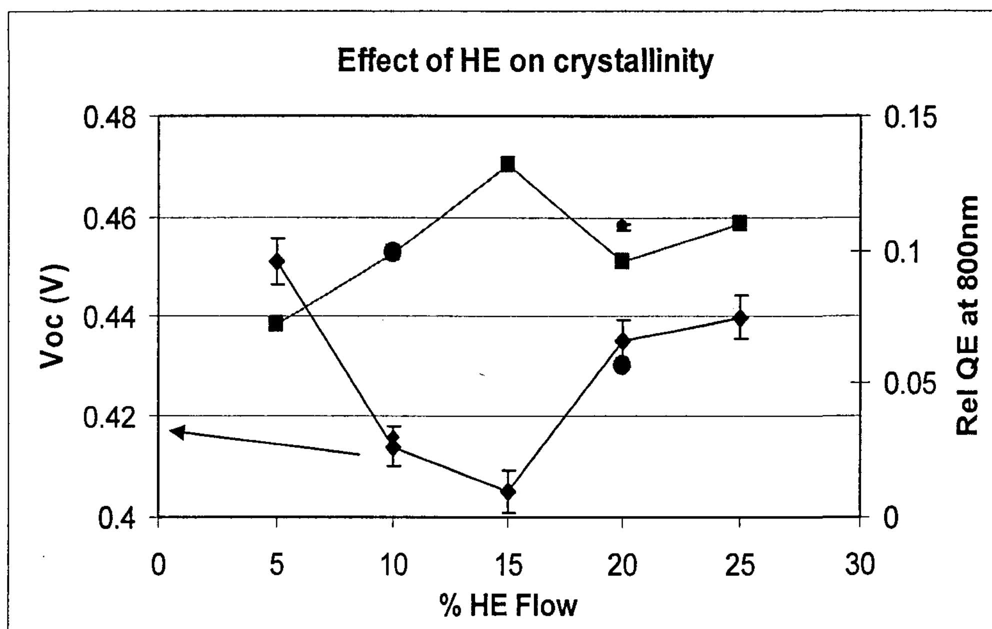

Figure [4.23]: Addition of HE changing crystallinity in different ways

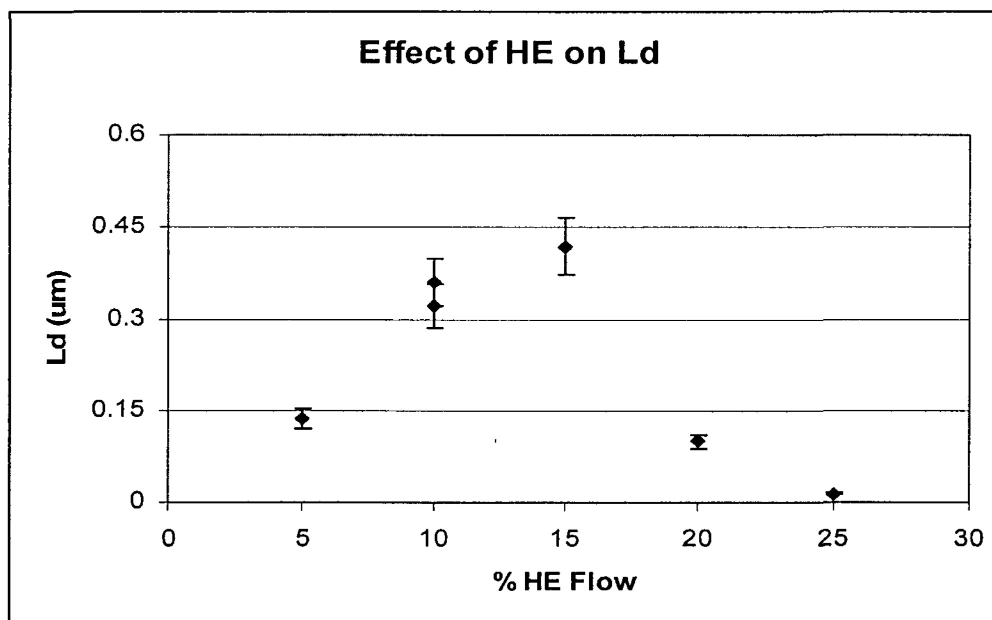

Figure [4.24]: Diffusion Length Vs. HE flow

2. Oxygen content and doping: Lower temperatures have been shown to lower the doping density in the devices.

The first factor would increase the current and decrease the voltage. The second factor would increase the current and fill factors, while the effect on voltage may not be as clear, since it would depend upon what happened to diffusion lengths and midgap defect densities. The previous work in the literature did not examine the effects of growth temperature on either defects or on diffusion length. In this work, we do so.

13. Influence of oxygen on device properties:

In Figure [4.25], we show the influence of deposition temperature on open circuit voltage and QE at 800 nm. The figure shows that Voc increases as the growth temperature is lowered, and the QE at 800 nm decreases. This is the case for both devices with and without seed layers. This is the expected result.

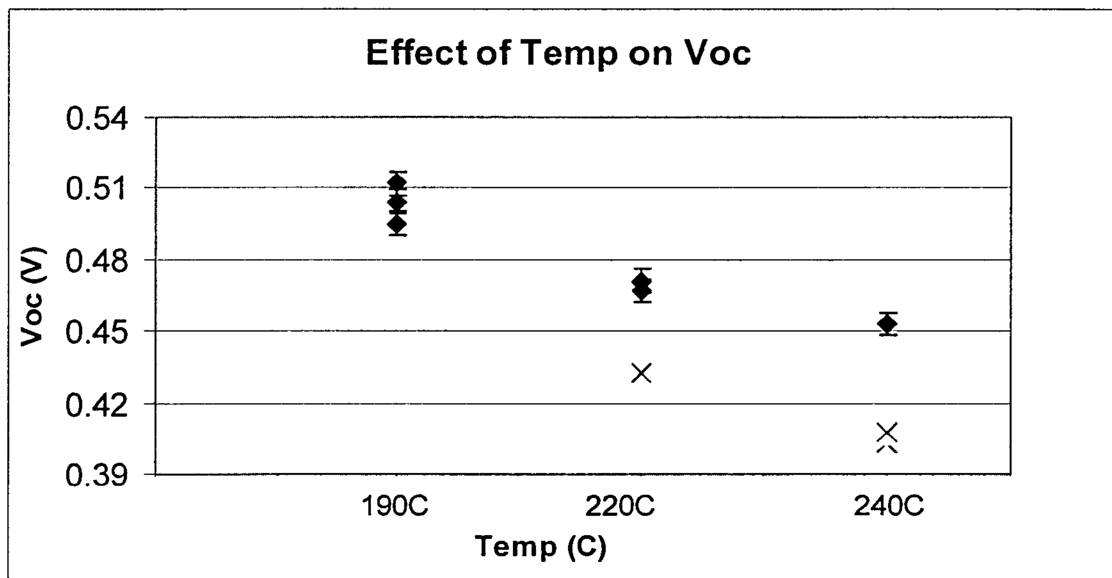

Figure [4.25]: Decreasing Temp leading to higher Voc

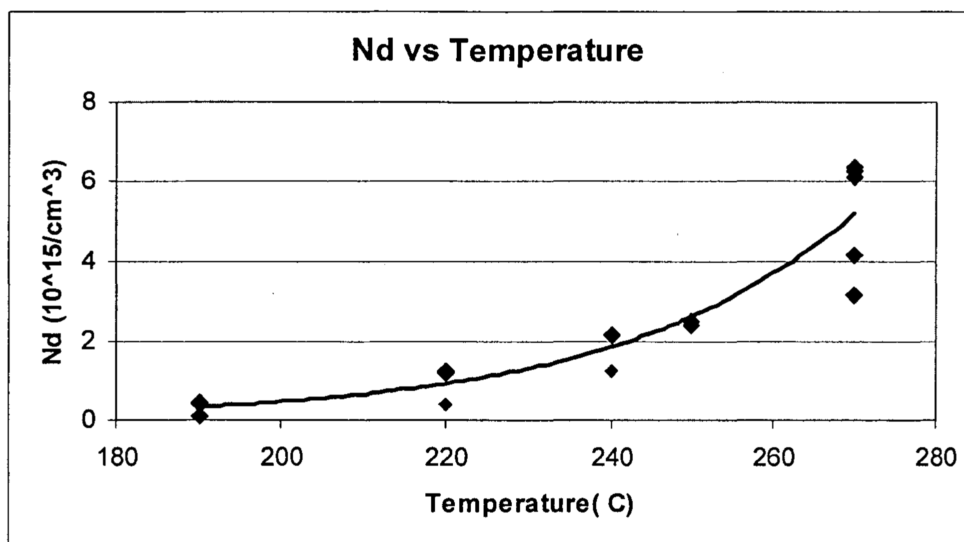

Figure [4.26] Doping Vs Temperature

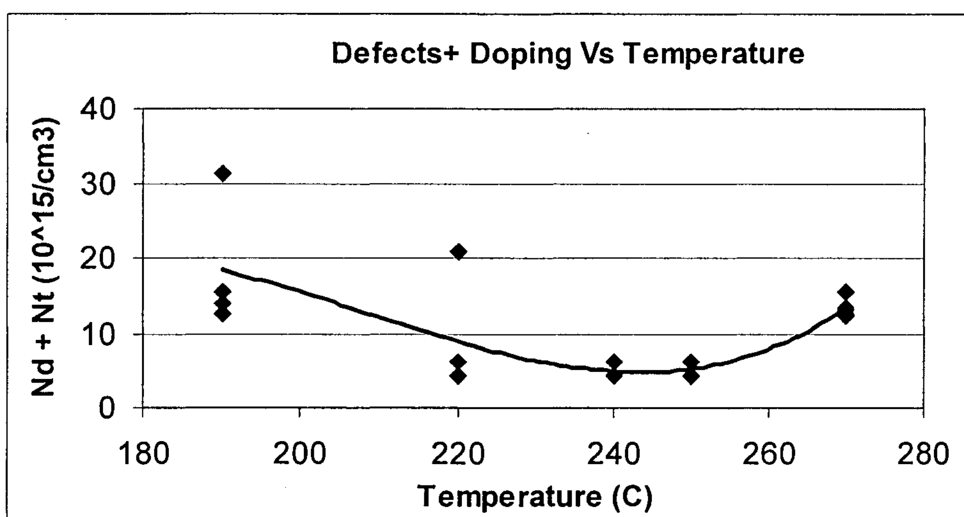

Figure [4.27] Doping & Defects Vs Temperature

In Figure [4.26], we show the result on doping density measured using capacitance on the deposition temperature. Very clearly, the doping increases at the growth temperature increases. This has been ascribed in past to more efficient doping of nc-Si: H by oxygen[40]. In

Figure [4.27], we show the data for defect densities, also as function of growth temperature. Unlike the case for doping, now at first, the defect density seems to decrease, and at higher values of doping, increase with doping. Thus, there is no longer a 1:1 correlation with doping, unlike the previous case where all the devices ere made at one temperature. The reason for anomalous behavior at the lowest temperatures may lie in the material being much more amorphous, and therefore, higher defect densities characteristic of amorphous Si, which are characteristically in the range of 10^{16} cm^{-3} at these lowest temperatures. It is well known that in a-Si: H, the lowest defect density is obtained in the range 240-270 C, and lower temperatures lead to higher defects. This effect needs further work.

14. Influence of baking of the reactor walls on defect densities:

In order to reduce the residual oxygen levels, it was decided to bake out the walls prior to deposition. The substrate was loaded in the chamber and then silane-hydrogen plasma was done, keeping the shutter closed so nothing deposited on the substrate. The objective of the plasma layer (dummy layer) was to getter impurities in the rector. Then the walls were baked out for 4 hours at ~ 120 C under vacuum in the reactor. Then the walls were cooled down using fans. The base pressure in the reactor reduced to below 1E-7 Torr, an order of magnitude decrease, after such bake out and dummy layer. Then another dummy layer was done for 45 minutes with the sample heating up to the desired temperature, and then the device layer was grown. In Figure [4.28] below, we show the results for the measured doping density for two different sets of samples. Each set corresponds to a different silane/hydrogen ratio during the growth of the nanocrystalline Si layer. It is seen that in each case, the baking of the walls led to a significant decrease in the doping density. Thus, reducing oxygen content in the reactor is critical for reducing doping and therefore, defect densities. Clearly, the ideal reactor system would be a load-locked reactor with multiple chambers so the inside of the n layer chamber does not see moisture except during the rare cleaning stages. We did not have such a reactor available for our work.

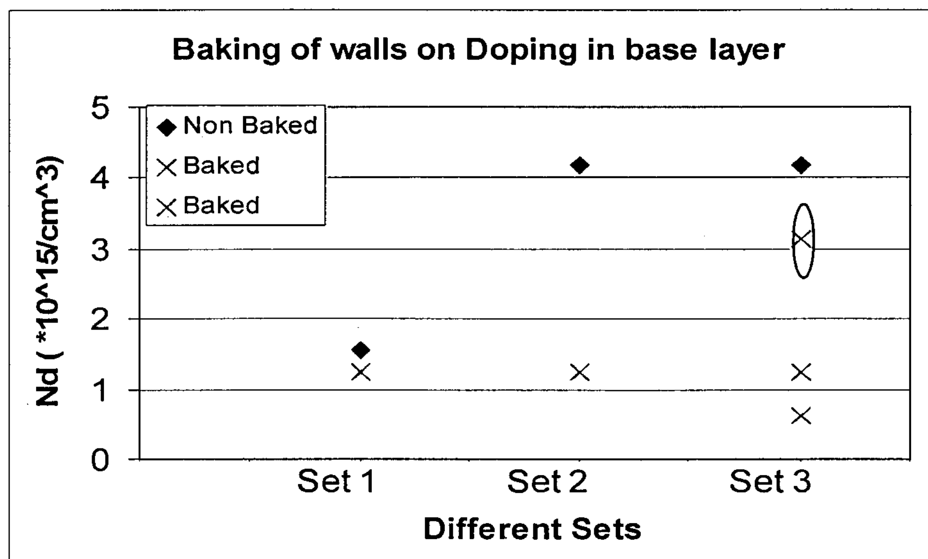

Figure [4.28]: Baking of reactor walls at 120C temperatures leading to lower oxygen

15. Other data relevant to this work:

While the above results are the ones that I obtained, I also provided samples to many other students for their complementary research projects. In particular, samples were provided to Dan Stieler for mobility measurements, and to Satya Saripalli for measurements of carrier lifetimes. Stieler measured electron mobilities using a n+nn+ geometry, and I was responsible for making some, though not all, n-type base layers. Saripalli measured hole lifetimes in the very same samples in which I had measured defect densities and diffusion lengths. He used a reverse recovery technique for measuring carrier lifetimes. The objective of the experiment was to see if the carrier lifetimes followed the inverse relationship to defect density, and by simultaneously measuring lifetime and diffusion length in the very same sample, one could obtain a measurement of carrier mobility, since diffusion length L and lifetime are related by the equation:

$$L = \text{sqrt}(D\tau) \quad \text{................ (4.2)}$$

where D is the diffusion coefficient of the minority carrier and τ is its lifetime. From the diffusion coefficient, one can evaluate mobility using the Einstein equation,

$$[D/\mu] = [kT/q] \qquad \text{........... (4.3)}$$

The data for lifetime vs. defect density are shown in Figure [4.29], showing an approximate linear relationship, thus confirming that SRH model is the appropriate model for recombination in this material. The hole mobility deduced from the simultaneous measurements of diffusion length and lifetimes is plotted in Figure [4.30], as a function of doping. One obtains a value of approximately 1 cm^2/V-s for hole mobility, in the same range as obtained recently by a group at Syracuse using time of flight techniques[41]. In contrast to their work, where they need a very low conductivity material, our technique allows for measurements in material with any doping, and is thus a superior technique. Also, we do not need to deconvolute difficult transient data, unlike their work. The mobility in Figure [4.30] is shown to decrease slightly with increasing doping.

This is the first such measurement of carrier lifetimes and mobilities in this important material.

Electron mobility in our materials was measured by Dan Stieler using space charge limited current techniques. His I-V data for one of our samples is shown in Figure [4.31], showing distinct ohmic and square law regimes, and the mobility deduced from the data is ~5 cm^2/V-s at 150 C . Further measurements on ours and other materials are in progress by him

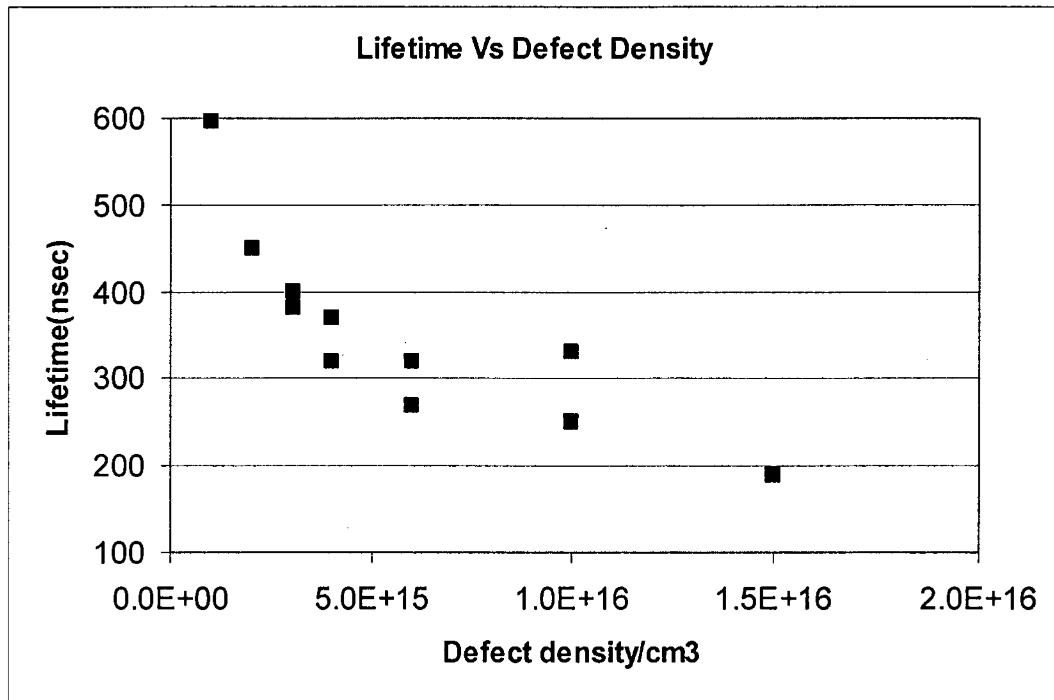

Figure *[4.29]: Lifetime Vs Defect Density*

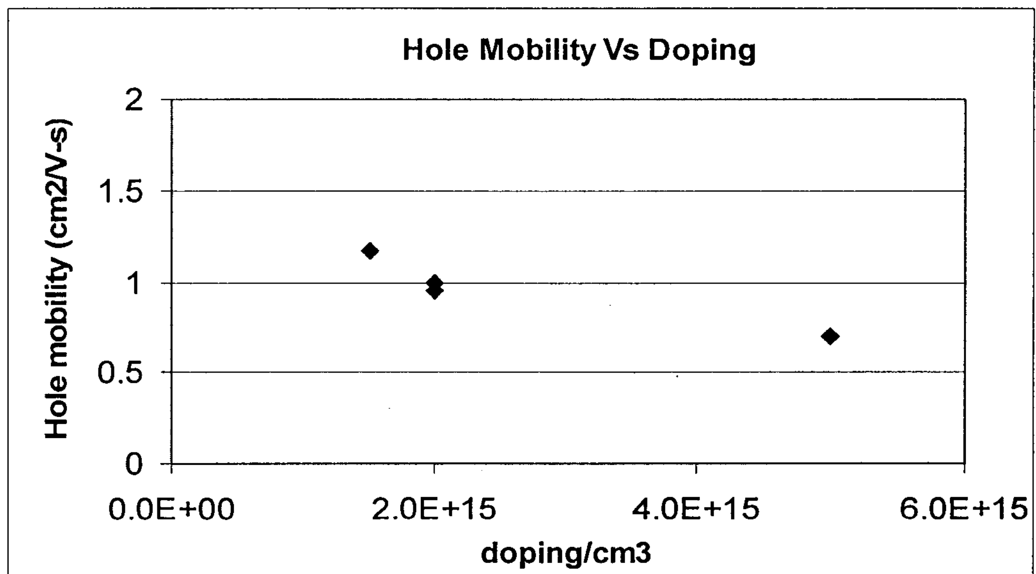

Figure [4.30]: Hole mobility Vs. Doping measured from the above measurement.

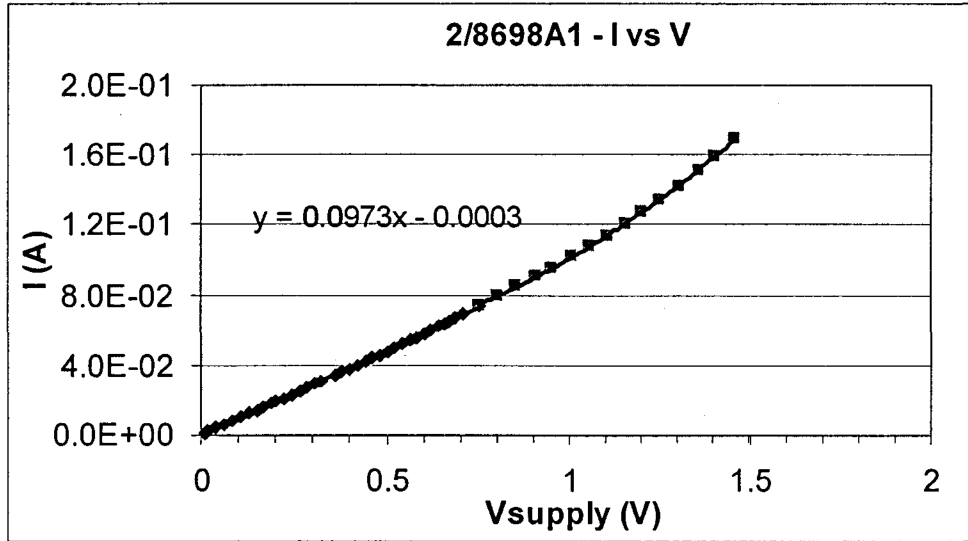

Figure [4.31]: IV curve for a n-i-n device

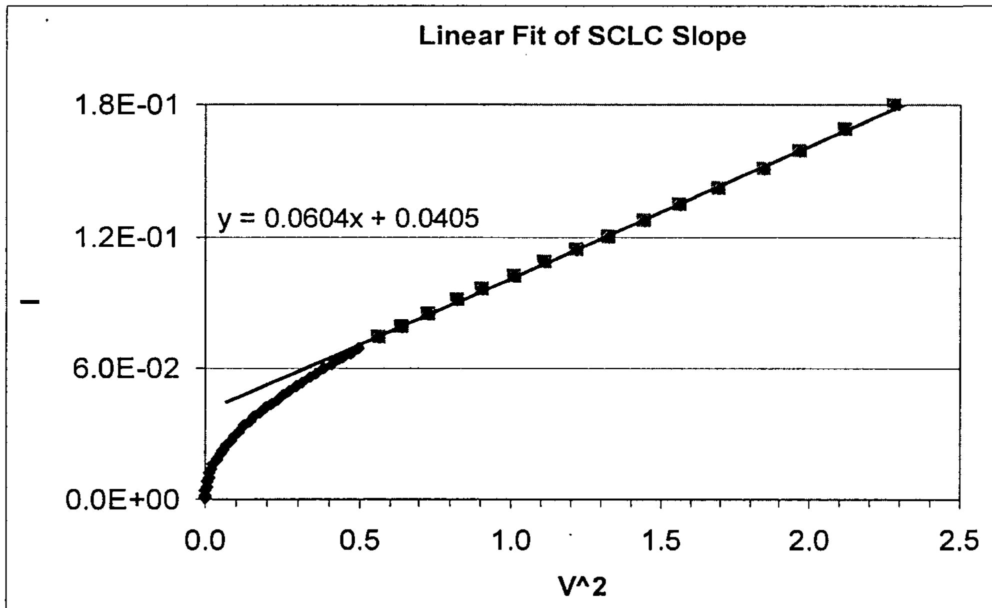

Figure [4.32] IV^2 for a n-i-n device at room temperature

CHAPTER 5

CONCLUSIONS

To conclude, a systematic study of fundamental material properties that affect device performance was undertaken in this work. The major results are as follows:

1) Both donor and deep level defect densities were measured in devices. The effective doping was varied using ppm levels of B / P to reduce / increase the n-type native doping. A surprising result was that there was a one-to-one correlation between the donor density and the deep defect density for samples that had a significant degree of crystallinity. This fact implies that the same element, probably oxygen, is responsible for creating both doping and defects.

2) The location of the traps was estimated using variable frequency capacitance techniques. The traps were found to be approximately 0.35 to 0.5 eV below the conduction band. This is the first time ever that both the density of defects and their energetic levels have been determined in this material in device-type structures.

3) Lowering the growth temperature led to lowering of donor densities. St the lowest growth temperatures, the amount of amorphous phase in the device increased, and the one-to-one relationship between the doping and defect densities was changed. The defect density now increased, since low temperature amorphous phase is known to have a high density of defects.

4) Lifetimes of minority carriers were measured in these very same devices, for the first time ever, by another student. A careful measurement of the defect densities by me and lifetimes by him revealed an inverse relationship between lifetime and defect density, suggesting that the SRH model for recombination was the dominant recombination mechanism.

5) Diffusion length of holes (minority carriers) was measured in the devices using a quantum efficiency technique. The diffusion length was shown to be inversely related

to the defect density, once again proving that the recombination was trap controlled with the SRH model being valid.

6) From the simultaneous measurement of diffusion length and lifetimes, one could estimate the mobility of holes in these devices. It was found to be in the range of ~ 1 cm^2/V-s. This is a new and relatively easy technique for measuring hole mobility, which is very difficult to measure using traditional methods such as time of flight.

7) Various novel device designs were utilized to improve devices. One technique was the use of graded doping with B which was shown to significantly improve carrier collection by inducing an internal electric field which helped transport of carriers.

8) Another novel technique to improve device performance was the use of an interfacial buffer or a-Si cap layer between the p+ and n layers. When appropriately designed, this buffer layer improved the open circuit voltage significantly.

9) Series resistance at the ITO/oxide interface was shown to be a major contributing factor for loss in fill factor. An Al buss-bar with annealing both by heat and with electrical drive-in reduced the series resistance by a factor of 2, and improved the fill factor to 69%.

10) It was shown that the addition of He during deposition could improve the device properties by changing the crystalline/amorphous ratios in a controlled manner.

11) It was shown that baking out of walls made a significant impact on the doping and defect densities, thus reiterating the important role of stray oxygen in introducing dopants and defects. It is recommended that a multi-chamber reactor be designed for further work.

FUTURE WORK

1. Future work should include studies of other materials such as (Si,Ge) and (Ge,C) so that the best solar cell device structures can be made.
2. Also methods for increasing the grain size while maintaining the low defect densities should be pursued.
3. Multi-chamber with ultra high vacuum should be set up to make high quality nc-Si: H samples
4. The relationship of these defects and crystallinity to some other measurements like Raman for devices and SIMS for oxygen in the samples should be studied.

REFERENCES

1. S. Veprek, V. Marecek, Solid State Electron. 11 (1968) 683
2. J. Meier, R. Fluckiger, et. al, Appl. Phys. Lett. 65 (7) (1994) 862-864
3. A. Shah, J. Meier et. E. Vallat, N. Wyrsch, U. Kroll, C. Droz, U. Graf, Solar Energy Materials & Solar Cells 78 (2003) 469-491
4. J. Kocka, et. al., Solar Energy Materials & Solar Cells 78 (2003) 493–512
5. L. Yang, L. Chen, S. Weideman, A. Catalano, MRS Symp. Proc. 283 (1993) 463.
6. H. Shirai, T. Arai, J. Non-Cryst. Solids, 198–200 (1996) 931.
7. J.K. Rath, F.D. Tichelaar, H. Meiling, R.E.I. Schropp, MRS Symp. Proc. 507 (1998) 879.
8. J. Kocka, A. Fejfar, et. al. MRS Symp. Proc. 557 (1999) 483.
9. F. Finger, J. Mcller, C. Malten, R. Carius, H. Wagner, J. Non-Cryst. Solids 266–269 (2000) 511.
10. M. Kondo, S. Yamasaki, A. Matsuda, J. Non-Cryst. Solids 266–269 (2000) 544.
11. J.H. Werner, N.E. Christensen, in: J.H. Werner, H.P. Strunk (Eds.), Polycrystalline Semiconductor II Springer, Proceedings in Physics Vol. 54 Springer Berlin 1991 p. 145
12. J.H. Werner, 13th ''Sunshine'' Workshop Technical Digest NEDO-PVTEC, Tokyo 2000 p. 41.
13. J. Kudrna, F. Trojanek, P. Mally, I. Pelant, Appl. Phys. Lett. 79 (2001) 626.
14. H. Takakura, Y. Hamakawa, Solar Energy Materials & Solar Cells 74 (2002) 479-487

15. R.W. Collins, A.S. Ferlanto, G.M. Ferrerira., C. Chen, J. Koh, R. Koval, Y. Lee, J. Pearce, C. Wronski, Solar Energy Materials & Solar Cells 78 (2003) 143–180
16. A. Shah, E. Vallat-Sauvain, P. Torres, J. Meier, U. Kroll, C. Hof, C. Droz, M. Goerlitzu, N. Wyrsch, M. Vanacek, Materials Science and Engineering B69–70 (2000) 219–226
17. X. Zhang, y. Zhu, F. Zhu, C.C. Wei, C. Wu, Y.Gao, J. Sun, G. Hou, X. Hua,S. Xiong , Applied Surface Science 245 (2005) 1-5
18. J. Meier, E. Vallat, S. Dubail, U. Kroll, J. Dubail, S. Golay, L. Feitknecht, P. Torres, S. Fay, A. Shah, Solar Energy Materials 66 92001) 73-84.
19. H. Curtins, N, Wyrsch, A. Shah, Electron Letters 23 (1987) 228
20. A.A. Howling, U. Kroll, F. Finger, J.Vac. Sci. Technology A 10 (1992)1080
21. S. Oda, J. Noda, M. Matsumura, Jpn. J. Appl. Phys. 29 (1990) 1889
22. A. Perret, P. Chabret, Appl. Phys. Lett. 86(2005) 021501
23. J.Dutta, U.Kroll, P.Chablor. and A.Shah, J. Appl. Phys. 72 (7) (1992) 3220
24. Yuan Min Li, Annual Technical Progress Report under Subcontract No. ZDJ-2-30630-28 (2002-2003)
25. J. Werner, Thin Solid Films 383 (2001) 95
26. Michio kondo, Solar Energy Materials & Solar Cells 78 (2003) 543–566
27. K. Yamamoto, A. Nakajima, M. Yoshimi, T. Sawada, S. Fukuda, T. Suezaki, M. Ichikawa, Y. Koi, M. Goto, T. Meguro, T. Matsuda, M. Kondo, T. Sasaki, Y. Tawada, Solar Energy 77 (2004) 939-949
28. L. C. Kimerling, J. of Appl. Phys. v 45 (1974) 1839-1845

29. V.L. Dalal, J.H. Zhu, M. Welsh and M. Noack IEEE Proc.-Circuits Devices Syst. Vol. 150 No. 4 (August 2003) 316-321

30. J, Zhu, V. Dalal, Materials Research Society Symposium - Proceedings v 762 (2003) 375-380

31. J. Meier, et.al. Solar Energy Materials & Solar Cells 66 (2001) 73-84

32. K. Lips, P. Kanshat, W. Fuhs, Solar Energy Materials and Solar Cells v 78 (2003) p 513-541

33. P. Kanschat, K. Lips, W. Fuhs, Hahn-Meitner-Institut, A. Hierzenberger, and R. Brüggemann, Institute für Physikalische Elektronik, Universität, . Mat. Res. Soc. Symp. Proc., Amorphous and Microcrystalline Technology (1998) A 13.4

34. V. Dalal , P. Sharma, Appl. Phys. Lett. 86 (2005) 103510

35. V. Dalal, P. Sharma, et al. Mat. Res. Soc. Symp. Proc. Vol. 808 A 8.2

36. M. Kondo, Journal of Non-Cryst. Solids, 266-269 (2000) 544-547

37. K. Yamamoto, A. Nakajima, et. al. Solar Energy 77 (2004) 939–949

38. N. Wang and V. Dalal, MRS Symp. Proc. Vol. 862 A 20.6.1

39. M. Konda, Solar Energy Materials and Solar Cells, 78 (2003) 543-566

40. J. H. Werner, R. Dassow, T.J. Rinke, J.R. Kohler, R.B. Bergmann, Thin Solid Films 383 (2001) 95-100

41. T. Dylla, F. Finger, E.A. Schiff, MRS Symp. Proc. Vol. 808 A 8.10.1

42. See, for example, B. Streetman and S. Banerjee, "Solid State Electronic Devices", 5th.Ed. (Prentice Hall, NY,2000) p. 3 (Appendix A)

ACKNOWLEDGEMENTS

First and foremost, I would like to express my sincere gratitude to my major professor, Dr. Vikram Dalal, for his invaluable guidance and support through out this research. I would like to thank him for being so closely involved with this project and making sure the research moves towards a purposeful direction.

I am also honored to have Dr. Gary Tuttle, Dr. Rana Biswas, Dr. Joe Shinar, and Dr. Mani Mina for being on my committee.

I would also like to thank Max Naock for his technical help and healthy discussions we had during this time. Lots of changes were made in VHF reactor during this time to make it consistent and a better quality system overall and Max played a big role at each step of these never ending modifications.

I would also like to thank Keqin Han, Jason Zhu, Matt Welsh, Nanlin Wang, and Satyalakshmi Sripalli for help with device deposition and characterization at different points of this project.

Also special thanks go to Jane Woline for helping me in all possible ways.

I would also like to thank my friends here at MRC - Durga Prasanna Panda, Dan Stieler, Debju Ghosh, Kamal Muthukrishnan, Andy Niu, and Vishwas Jaju and rest of the friends who always gave me good support.

Also very special thanks to my family without whose support this would not have been achieved.

And not the least, I would also like to thank NREL for funding this project.

APPENDIX A

Solving the transport equation for the holes traveling in the n layer by diffusion and from the depletion width after electron hole pairs have been generated with the light shining on the p+n .n+ device from the p side and assuming negligible thickness for the p layer We get the following equation[42].

$$J_p(y) = \frac{q\Gamma}{1-\alpha^{-2}L_d^{-2}} * \{([\frac{S}{\alpha D_p}+1]\cosh[\frac{y_0-y}{L_p}] - [\exp(-\alpha y_0)] * (\frac{S}{\alpha D_p}\cosh(\frac{y}{L_d}) + \frac{1}{\alpha L_p}\sinh(\frac{y}{L_d}))$$

$$* \frac{1}{(SL_p/D_p) * \sinh(\frac{y_0}{L_d}) + \cosh(\frac{y_0}{L_d})} - \exp(-\alpha y)\}$$

For y= y_0, we get

$$J_p(y_0) = \frac{q\Gamma}{1-\alpha^{-2}L_d^{-2}} * \{([\frac{S}{\alpha D_p}+1] - [\exp(-\alpha y_0)] * (\frac{S}{\alpha D_p}\cosh(\frac{y_0}{L_d}) + \frac{1}{\alpha L_d}\sinh(\frac{y_0}{L_d}))$$

$$* \frac{1}{(SL_d/D_p) * \sinh(\frac{y_0}{L_d}) + \cosh(\frac{y_0}{L_d})} - \exp(-\alpha y_0)\}$$

$$J_p(y_0) = \frac{q\Gamma}{1-\alpha^{-2}L_d^{-2}} * \{(1 - [\exp(-\alpha y_0)] * \frac{1}{\alpha L_d}\sinh(\frac{y_0}{L_d})) * \frac{1}{\cosh(\frac{y_0}{L_d})} - \exp(-\alpha y_0)\}$$

As we know α (absorption coefficient) is small for indirect band gap nc-Si at wavelength of 900 nm and αy_0 is very small, we assume exp (- αy_0) ~ equal to 1

Here L_d is the total distance that the hole travels before getting collected which is equal to depletion width Wd and diffusion length of hole Lp.

$$J_p(y_0) = \frac{q\Gamma}{1-\alpha^{-2}L_d^{-2}} * (1 - \frac{1}{\alpha L_d})$$

As Quantum Efficiency = $J_L(\lambda)/ q\Gamma(\lambda)$ and solving the above equation we find that

$$QE = \alpha (Lp + Wd)$$

only when thickness of n layer is bigger than the depletion width, surface recombination and thickness of p layer can be neglected.

APPENDIX B

Mat. Res. Soc. Symp. Proc. Vol. 808 2004 Materials Research Society **A.8.2.1**

Defect Densities, Diffusion Lengths and Device Physics in Nanocrystalline Si:H Solar Cells

Vikram L. Dalal*, Puneet Sharma*, David Staab, Max Noack+ and Keqin Han+

* Iowa State University, Dept. of Electrical and Computer Engr. and Microelectronics Research Center, Ames, Iowa 50011, USA

+ Iowa State University, Microelectronics Research Center, Ames, Iowa 50011,USA

ABSTRACT

We report on the properties of nanocrystalline Si:H solar cells. The solar cells were of the p+nn+ type, with the n+ layer deposited first on a stainless steel substrates. The solar cells were prepared under high hydrogen dilution conditions using either ECR plasma deposition, or VHF diode plasma deposition processes. The deposition pressures were kept low, 5 mTorr in the ECR reactor and 50 mTorr in the VHF reactor. All the solar cells reported showed a high Raman ratio of crystalline to amorphous peaks. Properties such as dark current, deep level defects and shallow doping densities, and hole diffusion lengths were measured in these cells. It was found that the base layer was always n type, but that its doping could be changed by adding ppm levels of B during growth. A sufficient B doping even type converted the base layer to p type. It was found that there was a good one-to-one correlation between the shallow doping and deep level defects, suggesting that the same element, probably oxygen, is responsible for generating both shallow dopants and deep levels. The diffusion length of holes was measured in these cells using quantum efficiency vs. voltage techniques, and it was found that the diffusion length data could be explained very well by invoking trap-controlled recombination statistics. The dark I(V) curves could be represented by a standard diode model for highly crystalline materials, but as the degree of crystallinity was reduced, the diode factor increased. Voltage could be improved by reducing the crystallinity of the layer,

but doing so resulted in a decrease in quantum efficiency in the infrared regions of the solar spectrum.

INTRODUCTION

Nanocrystalline Si:H, with grain sizes of the order of 10-20 nm, is an attractive materials for solar energy conversion [1-5]. It is known that H is present in this material, mainly at the grain boundaries, and also, there may be a thin amorphous Si:H tissue surrounding the small grains [6]. The presence of hydrogen seems to passivate the grain boundaries, reducing recombination of minority carriers at the boundaries. Solar conversion efficiencies approaching 10% have already been achieved in this material system, and when combined with a-Si:H as a top cell, efficiencies in excess of 14% has been reported [1].

In this paper, we will investigate the device physics of nanocrystalline Si:H solar cells by measuring the fundamental properties of the materials in devices, and then correlating these properties with the expected device results. The properties measured include doping, deep level defects, hole diffusion length, and dark I(V) curves.

FABRICATION OF DIAGNOSTIC DEVICES

The diagnostic devices were of the p_+nn_+ type, with the n_+ layer deposited first on a stainless steel substrate. No special back reflector was used. A transparent ITO contact was used on the p_+ layer. Thin buffer layers were used at both the n_+n and p_+n interfaces to limit interface recombination [5,7]. The buffer layers were a-Si:H at the back (between n_+ and n), and a thin, graded gap a-(Si,C):H layer at the p_+n interface. The doped layers were deposited using the ECR process, whereas the undoped base layer, generally n type, was deposited using either the ECR process described previously, or a VHF diode process at 45 MHz. Care was taken to prevent cross-contamination between layers. For example, for the cells made using VHF process, two separate reactors, one for doped, and one for undoped layers, were used. The undoped base layer was deposited in two stages, a nucleation stage where a hydrogen/silane ratio of 20:1 was used, and a further stage where the ratio was reduced to 12:1 to 14:1. Raman spectra were obtained on some of the devices, which clearly showed highly crystalline base layers, with a Raman peak ratio (ratio of peak at 520 cm_{-1} to the peak at 480 cm_{-1})of ~3.8:1 or higher.

The growth temperature for the base layer was kept low, ~300 °C, so as to preserve hydrogen bonding at both grain boundaries and in the a-Si:H tissue. Use of temperatures in excess of 350 °C generally resulted in a poorer device.

RESULTS ON DIAGNSOTIC DEVICES

Fig. 1 shows a typical I(V) curve for a device made using the VHF process without any special back reflector. The current density is 12 mA/cm^2, the voltage is 0.47V and the fill factor is 0.65. The n layer thickness was ~1.2 micrometer. The corresponding quantum efficiency curve is shown in Fig.2.

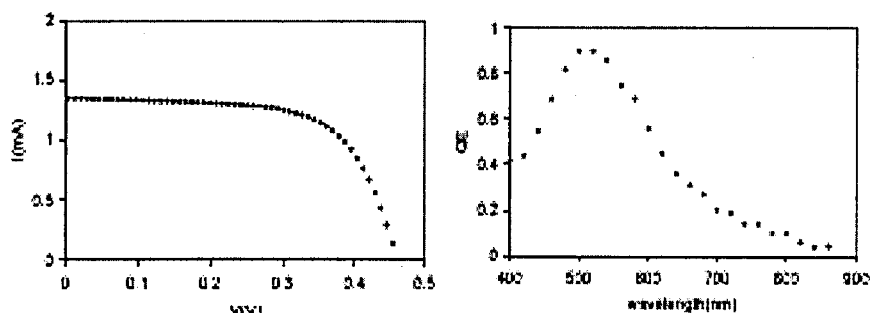

Fig. 1 I-V curve of diagnostic device   Fig.2 QE of sample whose I-V curve is in Fig. 1

MEASUREMENT OF DEFECT AND DOPING DENSITIES

The devices were subjected to C-V measurements at various frequencies. In Fig. 3, we show the results of such measurements, plotted as $1/C^2$ vs V at various frequencies. A feature to notice is that all 4 curves in the figure are approximately parallel at low voltages, but the curves at higher frequencies tend to saturate in reverse voltage, implying that the depletion depth in the base layer has reached the $n+$ contact. This behavior is easily explained by invoking Kimerling's model[8], where the data at low voltages correspond to the shallow state density (donor states), but the data at high voltages and low frequencies correspond to the sum of (doping + deep level) densities. From such considerations, we can evaluate the shallow-state (doping density) to be ~ 7.5 x10^{15}/cm^3, and the sum of shallow and deep state doping to be 1.6x10^{16}/cm^3. Thus, the deep state defect density is ~8.5x10^{15}/cm^3, in the same

range as the doping density. Such a correlation between deep states and donor states was also seen in the work of Lips et al [9].

It was found that both donor and deep state densities could be varied by compensating with B. Upon adding B, donor density decreased, and so did the deep defect density. This relationship is shown in Fig. 4. This relationship implies that most likely, the same element is responsible for creating both donor and deep states. We speculate that this element is oxygen. The reason B reduces both shallow donors and deep defects is because it complexes with oxygen, removing its levels from the bandgap, in a way similar to its complexing with oxygen in crystalline Si.

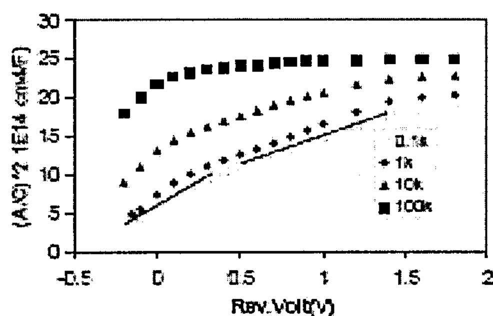

Figure [3] Behavior of CV as a function of frequency

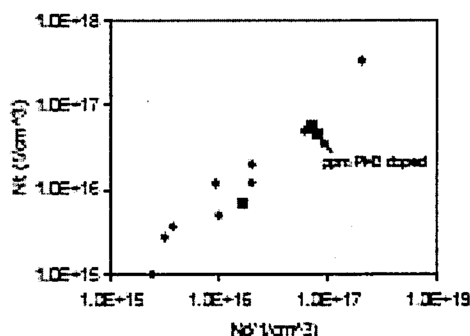

Figure [4]: Deep level defect density vs. donor density.

Note that the C-V curves plotted in Fig. 3 actually yield information about where in energy the deep levels are. The energetic position of the deep levels can be estimated by studying the frequency behavior. At the highest frequencies used (100 kHz), the capacitance curve saturates at about 0.7 V in reverse bias, which says that the depletion width has equaled the thickness of the n layer. The saturated capacitance value yields a n layer width of 0.55 micrometer for this particular cell, in very good agreement with the width calculated from reflection data on the cell. If one now uses the doping density ($7.5x10_{15}/cm_3$), one obtains, at a reverse bias of 0.7 V, a depletion width of 0.53 micrometer (assuming a built-in voltage of 0.8 V), in excellent agreement with the above two values. Thus, capacitance data shown in Fig. 3 is self consistent. The data also show that deep states have ceased to respond at 100

kHz. That fact gives us a value of (Ec-Et) of 0.35 eV as the upper limit for trap position. The lower limit can be evaluated from observing when the capacitance begins to decrease with frequency, which is shown in Fig. 5. From that figure, we conclude that the deepest states must have (Ec-Et) ~ 0.5

eV. Both these numbers are calculated using the usual formula for attempt to escape frequency, $\nu = \nu_o \exp[-(Ec- Et)/kT]$ where ν_o is ~1×10^{11}/sec. Using an upper estimate of ν_o (e.g. 1×10^{12}/s) changes the numbers for the trap energy only slightly, given the logarithmic relationship between energy and ν_o.

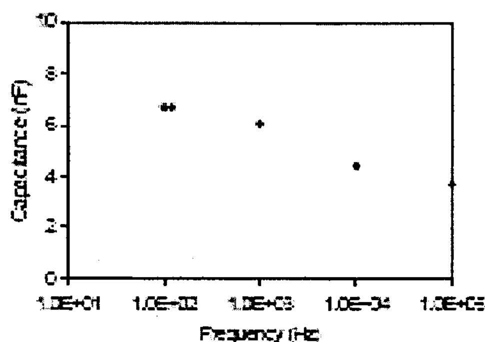

Figure [5] Capacitance vs. Frequency at 0 bias

MEASUREMENT OF DIFFUSION LENGTH OF HOLES

The diffusion length of holes was measured using quantum efficiency vs. voltage techniques, in combination with capacitance-voltage measurements. It is known [10] that when $\alpha L \ll 1$ and $t/L \ll 1$, where α is the absorption coefficient, and t the thickness of the undepleted base layer, and L the diffusion length , QE ~ $\alpha (w_d + L)$. Here, w_d is the depletion width. By applying a voltage, one changes the depletion width, which is determined from the low frequency capacitance value. By plotting relative QE signal, measured at 900 nm, vs. w_d, the intercept gives an estimate of diffusion length. Such a measurement is shown in Fig. 6 for two cells, one with a high doping (and defect) density, and one with a low doping (and defect) density. The intercepts yield values of 0.57 and 1.2 micrometer for L for the two samples. The square of the measured diffusion length is plotted against 1/(defect density) in Fig. 7, and it shows a linear relationship over two orders of magnitude in defect density, as

expected from a simple trap-controlled recombination model, if we assume that the mobility value is relatively independent of doping, a reasonable assumption in small grained materials where mobility is mainly controlled by transport across grain boundaries.

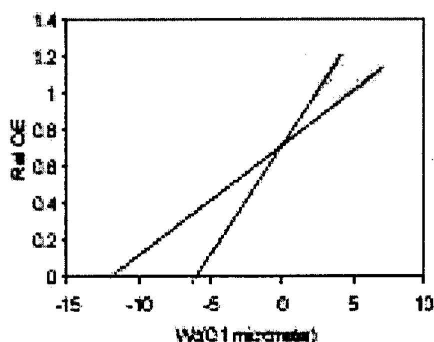

Figure [6] Diffusion length estimated from measurement of QE vs. voltage which changes diffusion length.

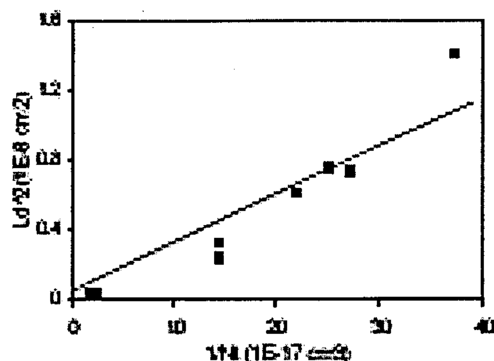

Figure [7] Square of diffusion length vs. inverse of defect density

MEASUREMENT OF DARK I-V CURVES

We observed two distinct types of dark I-V behavior. In samples made using the ECR process, one almost always observed an I-V curve characteristic of a standard, two-region, exp(qV/2kT) and exp(qV/kT) type behavior. In contrast, in samples prepared using VHF, we observed a more homogeneous exp(qV/nkT) behavior, with n values around 1.5. See Fig. 8 and 9. The differences can be traced to the different degrees of crystallinity between the films produced in the two reactors. The ECR reactor almost always produced films with a high degree of crystallinity (high Raman ratios, ~6:1 or greater) whereas the VHF reactor produced films with a significantly lower degree of crystalline/amorphous ratio (3.5:1). When the sample becomes more amorphous, of course, the dark I(V) curve becomes dominated by a distribution of states in the bandgap, with a n factor approaching 1.5. The capacitance data for VHF samples clearly shows a distribution of states between 0.35 and 0.5 eV below conduction band edge and so it is not a surprise that such samples do not show the classical n=1 and n=2 I-V behavior. This conclusion is supported by examining the I-V curve for a sample whose crystallinity was deliberately degraded by adding He to the ECR reactor during growth. The resulting Raman signal showed a significantly increased shoulder at 480

cm-1 compared to the sample produced without adding any He to the discharge. The resulting dark I-V curve had the same shape as the one shown n Fig. 9, confirming that it is the degradation of crystallinity which causes the dark IV curve to assume a non-ideal form. A consequence of the increase in amorphous phase is the increase in voltage, but a decrease in QE at 800 nm, as reported previously [5].

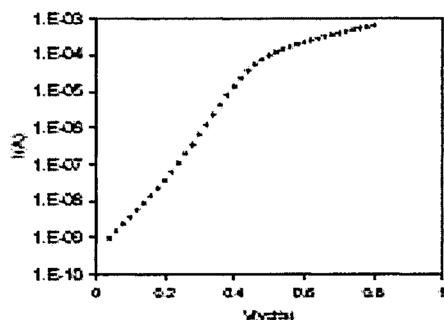

Figure [8] Dark IV of a sample prepared in ECR reactor showing two distinct exp (qV/2kT) and exp (qV/kT) behavior

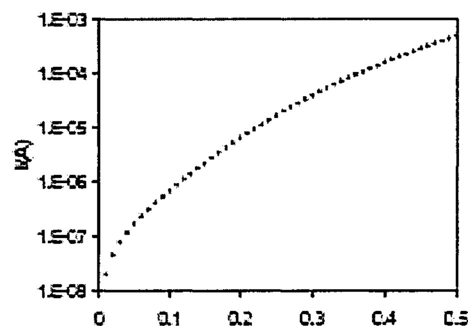

Figure[9] Dark IV of a sample prepare in VHF reactor showing single n factor.

CONCLUSIONS

In conclusion, this work has shown that there is a distribution of deep states in most nanocrystalline Si:H samples, located about 0.35 to 0.5 eV below the conduction band. There seems to be a distinct correlation between doping density and deeper defect densities. The transport of holes is controlled by diffusion, and the diffusion length can be related very well to the inverse of the deep state density. The defect density can be reduced by compensating with B, with a corresponding increase in diffusion length. The dark I-V curve depends greatly upon the degree of crystallinity of the sample, with highly crystalline samples producing classical two region dark I-V curves, but samples with a greater degree of amorphous phase producing I-V curves with a n factor closer to 1.5.

ACKNOWLEDGEMENT

The work was partially supported by NSF and NREL. We thank D. Panda, Nanlin Wang and Debju Ghosh for their technical help.

REFERENCES

1. Kenji Yamamoto, Masashi Yoshimi, Yuko Tawada, Susumu Fukuda, Toru Sawada, Tomomi Meguro, Hiroki Takata, Takashi Suzuki, Yohei Koi, Katsuhiko Hayashi Solar Energy Mater. And Solar Cells, 74, 449-455 (2002)
1. B. Rech, O. Kluth, T. Repmann, T. Roschek, J. Springer, J. Müller, F. Finger, H. Stiebig and H. Wagner , Solar Energy Mater. And Solar Cells, 74, 439-447(2002)
2. J. Meier, S. Dubail, S. Golay, U. Kroll, S. Faÿ, E. Vallat-Sauvain, L. Feitknecht, J. Dubail and A. Shah, Solar Energy Mater. And Solar Cells, 74, 457-467(2002)
3. A. V. Shah, J. Meier, E. Vallat-Sauvain, N. Wyrsch, U. Kroll, C. Droz and U. Graf, Solar Energy Mater. And Solar cells, 78, Pages 469-491 (2003)
4. V. L. Dalal, Jianhua Zhu, Max Noack and Matt Welsh, IEE Proc.-Circuits and Devices, 150, 316(2003)
5. R. Biswas and B. C. Pan, Proc. Of Mater. Res. Soc., 762, 15 (2003)
6. V. L. Dalal and K. Erickson , Proc. Of Mater.Res.Soc , Vol. 609(2000)
7. L. C. Kimerling, Journal of Applied Physics, v 45, p 1839-1845 (1974)
8. K. Lips, P. Kanshat, W. Fuhs, Solar Energy Mater. and Solar Cells, v 78, p 513-541(2003)
9. See, for example, B. Streetman and S. Banerjee, "Solid State Electronic Devices", 5th. Ed., (Prentice Hall, NY,2000), p. 3